

## Article

# Insights into the Corrosion Inhibition Performance of Isonicotinohydrazide Derivatives for N80 Steel in 15% HCl Medium: An Experimental and Molecular Level Characterization

Abdelkarim Ait Mansour <sup>1</sup>, Badr El-Haitout <sup>1</sup>, Raihana Jannat Adnin <sup>2</sup>, Hassane Lgaz <sup>3,\*</sup>, Rachid Salghi <sup>1</sup>, Han-seung Lee <sup>4,\*</sup>, Mustafa R. Alhadeethi <sup>5</sup>, Mouslim Messali <sup>6</sup>, Khadija Haboubi <sup>7</sup> and Ismat H. Ali <sup>8</sup>

- <sup>1</sup> Laboratory of Applied Chemistry and Environment, ENSA, University Ibn Zohr, P.O. Box 1136, Agadir 80000, Morocco
  - <sup>2</sup> Department of Smart City Engineering, Hanyang University ERICA, 55 Hanyangdaehak-ro, Sangrok-gu, Ansan-si 15588, Gyeonggi-do, Republic of Korea
  - <sup>3</sup> Innovative Durable Building and Infrastructure Research Center, Center for Creative Convergence Education, Hanyang University ERICA, 55 Hanyangdaehak-ro, Sangrok-gu, Ansan-si 15588, Gyeonggi-do, Republic of Korea
  - <sup>4</sup> Department of Architectural Engineering, Hanyang University ERICA, 55 Hanyangdaehak-ro, Sangrok-gu, Ansan-si 15588, Gyeonggi-do, Republic of Korea
  - <sup>5</sup> Department of Chemistry, College of Education, Kirkuk University, Kirkuk 36001, Iraq
  - <sup>6</sup> Department of Chemistry, College of Science, Imam Mohammad Ibn Saud Islamic University, P.O. Box 90950, Riyadh 11623, Saudi Arabia
  - <sup>7</sup> Engineering Science and Application Laboratory (LSIA), National Institute of Applied Sciences of Alhoceima, University Abdlmalk Essadi-Tetouan, Tétouan 93000, Morocco
  - <sup>8</sup> Department of Chemistry, College of Science, King Khalid University, P.O. Box 9004, Abha 61413, Saudi Arabia
- \* Correspondence: hlغاز@hanyang.ac.kr (H.L.); ercleehs@hanyang.ac.kr (H.-s.L.)



**Citation:** Ait Mansour, A.; El-Haitout, B.; Adnin, R.J.; Lgaz, H.; Salghi, R.; Lee, H.-s.; Alhadeethi, M.R.; Messali, M.; Haboubi, K.; Ali, I.H. Insights into the Corrosion Inhibition Performance of Isonicotinohydrazide Derivatives for N80 Steel in 15% HCl Medium: An Experimental and Molecular Level Characterization. *Metals* **2023**, *13*, 797. <https://doi.org/10.3390/met13040797>

Academic Editors: Anthony Hughes, Anthony Somers and Hannu Hänninen

Received: 20 January 2023  
Revised: 30 March 2023  
Accepted: 12 April 2023  
Published: 18 April 2023



**Copyright:** © 2023 by the authors. Licensee MDPI, Basel, Switzerland. This article is an open access article distributed under the terms and conditions of the Creative Commons Attribution (CC BY) license (<https://creativecommons.org/licenses/by/4.0/>).

**Abstract:** In this work, two compounds of isonicotinohydrazide organic class, namely (*E*)-*N'*-(1-(4-(dimethylamino)phenyl)ethylidene) isonicotinohydrazide (MAPEI) and (*Z*)-*N'*-(2-oxo-2, 3-dihydro-1H-inden-1-ylidene) isonicotinohydrazide (OHEI) were synthesized and evaluated for corrosion protection of N80 steel in a concentrated acidic medium (15 wt.% HCl) at a temperature of 303 K. The weight loss method (gravimetric method) and electrochemical techniques, i.e., electrochemical impedance spectroscopy (EIS) and potentiodynamic polarization curves (PPC), were used to evaluate the inhibition and adsorption characteristics of tested compounds. Further, surface characterization using a scanning electron microscope (SEM) was used to assess the surface morphology of steel before and after inhibition. Weight loss experiments at 303 K and 363 K showed that tested compounds' performance decreased with the increase in temperature, particularly at low concentrations of inhibitors whereas they exhibited good stability at higher concentrations. Electrochemical tests showed that MAPEI and OHEI inhibitors were effective at  $5 \times 10^{-3}$  mol/L, reaching an inhibition efficiency above 90%. It was also determined that the adsorption of both inhibitors followed the Langmuir adsorption isotherm model. Furthermore, SEM analysis showed that the investigated compounds can form a protective layer against steel corrosion in an acidic environment. On the other hand, the corrosion inhibition mechanism was established from density functional theory (DFT), and the self-consistent-charge density-functional tight-binding (SCC-DFTB) method which revealed that both inhibitors exerted physicochemical interactions by charge transfer between the s- and p-orbitals of tested molecules and the d-orbital of iron. The results of this work are intended to deepen the research on the products of this family to control the problem of corrosion.

**Keywords:** corrosion inhibitor; isonicotinohydrazide; N80 steel; weight loss method; DFT; molecular dynamics; SEM

## 1. Introduction

Corrosion is one of the biggest problems in industries that is affecting metallic materials (steel, copper, iron, . . . ). The N80 steel is one of the most important metals in the oil industry because it is cheap, strong, and resistant to various environmental phenomena, and also has very important physical and mechanical properties [1–3]. Acid solutions such as 15–28% HCl are used in industries for the acidization process when transporting gas and oil in steel pipes to increase productivity. In this process, acid solutions attack the metal equipment and cause serious corrosion [4–6]. Thus, different procedures are needed to protect this metal from corrosion. In this regard, one of the cheaper and more effective methods to protect this metal is the addition of corrosion inhibitors to the acidic solution [7–10]. Based on the chemical nature of compounds, there are two classes of inhibitors, organic and inorganic; however, most effective inorganic compounds are dangerous and toxic to the environment. Many classes of organic compounds, however, are not dangerous and are eco-friendly and effective for protecting against metal corrosion, especially compounds that contain aromatic rings, heteroatoms such as N, O, or P, and  $\pi$ -systems [9,11–13].

Hydrazides are among the most used organic classes that are still in continuous interest due to their diverse and wide spectrum of biological and chemical applications [14,15]. Hydrazides are also versatile intermediates and starting materials for the preparation of a variety of heterocycles [16,17]. In corrosion inhibition studies, hydrazide derivatives have been widely exploited as important compounds for corrosion mitigation in various corrosive mediums. In a recent review, Prakash Shetty eloquently reported a number of uses of hydrazide derivatives as corrosion inhibitors of steels in different corrosive solutions [18]. Hydrazide compounds such as acetohydrazides, benzo hydrazide, azelaic acid dihydrazide, and leochemical-based hydrazides showed excellent corrosion inhibition properties for steel in acidic mediums [18].

Isonicotinohydrazides are used in biology in a variety of fields, including as a commercial drug for the prevention and treatment of tuberculosis, and also used as one of the best corrosion inhibitors because of their good anticorrosion properties [19–21]. More recently, Abd EL-Lateef et al. [22] reported the application of a novel nicotinohydrazone Schiff base ligand and its complexes with Zn(II) and ZrO(II) for corrosion protection of mild steel in 1.0 mol/L HCl. The 5-sodium sulfonate-2-hydroxybenzylidene)nicotinohydrazone (H<sub>2</sub>LCs) and its complexes showed excellent corrosion inhibition abilities with the ZrO(II) complex (ZrOLCs) having the highest inhibition efficiency of 97.4% at  $5 \times 10^{-4}$  mol/L. In a recent study that tested the efficacy of Isonicotinohydrazide-based Schiff bases for J55 steel corrosion in 5% (w/v) HCl at various temperatures, Iroha and Dueke-Eze [23] reported an inhibition efficiency of 94.2% and 93.5% at 0.8 mmol/L of N-(5-nitro-2-hydroxybenzylidene)isonicotinohydrazide (N<sub>5</sub>N<sub>2</sub>-HBI) and N-(2-hydroxybenzylidene)isonicotinohydrazide (N<sub>2</sub>-HBI), respectively. The authors concluded that both compounds acted by blocking both anodic and cathodic corrosion reactions with a dominant anodic effect. In spite of these studies, research that has sought to investigate the corrosion inhibition characteristics of Isonicotinohydrazides for steels in highly acidic mediums is not reported. To the best of the authors' knowledge, the study presented in this article is the first attempt to assess the corrosion inhibition properties of Isonicotinohydrazides for N80 steel in 15 wt.% HCl medium.

On the other hand, it has been proved that the corrosion inhibition process is a complex phenomenon that cannot be easily understood from only experimental studies. In this context, great efforts have been made to implement computational methods to investigate the adsorption characteristics of organic compounds on metal surfaces. Quantum chemical calculations are one of the classical methods to study the electronic and structural properties of organic compounds, aiming to provide a better explanation of their corrosion inhibition characteristics [24–26]. However, this approach is very limited in describing the interaction with metal surfaces including bond formation and breaking upon adsorption, which is an essential criterion for simulating the corrosion inhibition process by organic compounds. To overcome this limit, other methods such as first-principles density functional theory

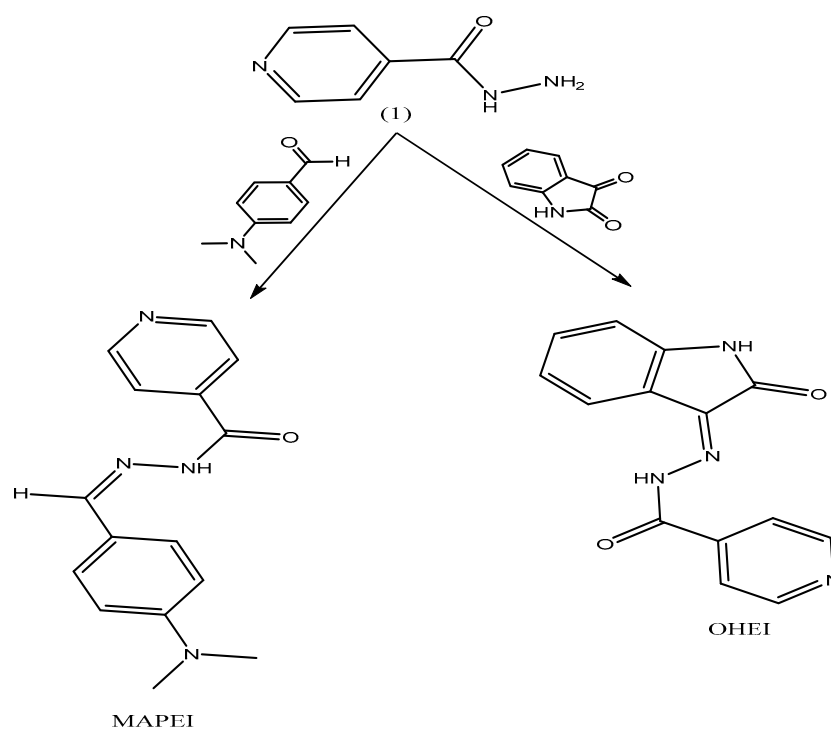
(DFT) and self-consistent-charge density-functional tight-binding method (SCC-DFTB) are needed to obtain more realistic insights into the corrosion inhibition process [27].

Herein, to understand the effect of the two compounds under investigation, i.e., (*E*)-*N'*-(1-(4-(dimethylamino) phenyl) ethylidene) isonicotinohydrazide (MAPEI) and (*Z*)-*N'*-(2-oxo-2,3-dihydro-1H-inden-1-ylidene) isonicotinohydrazide (OHEI) on the corrosion process of N80 steel in 15 wt.% HCl solution, several experimental tests were performed such as gravimetric analysis (WL), electrochemical impedance spectroscopy (EIS), and potentiodynamic polarization (PDP) methods. Furthermore, a scanning electron spectroscopy (SEM) was used to evaluate the morphology of the N80 steel with and without inhibitors. In addition, to explore further the inhibition mechanism, a comprehensive theoretical study was conducted using density functional theory (DFT), and the self-consistent-charge density-functional tight-binding method (SCC-DFTB). Thus, deep insights into the nature of interactions between tested compounds and the iron surface were obtained.

## 2. Materials and Methods

### 2.1. Materials and Samples

The N80 steel samples were purchased from local manufacturer in Casablanca, Morocco. N80 steel as the working electrode had the following weight percentages: 0.31%C, 0.19Si, 0.01%P, 0.008%S, 0.02Cr, and the rest used was Fe. The dimensions of the N80 steel used for gravimetric and electrochemical methods (EIS and PPC) were (4 cm × 2.3 cm × 0.3 cm) and (1.5 cm × 1.2 cm × 0.4 cm), respectively. This electrode was rubbed with abrasive paper (180–1200), cleaned with deionized water and ethanol, and air dried. The 15 wt.% HCl solution was prepared from a commercial chloride acid solution (37% HCl). Corrosion inhibitors were synthesized using the following procedure and Scheme 1:



**Scheme 1.** Synthesis procedure for MAPEI and OHEI compounds.

Synthesis of *N'*-(*Z*)-[4-(dimethylamino)phenyl]methylidene]pyridine-4-carbohydrazide (MAPEI): In a 50 mL (RBF), a mixture of 0.01 mmole of isoniazide (1) and 0.01 mmole of 4-(dimethylamino)benzaldehyde with few drops of glacial acetic acid in 25 mL of absolute ethanol was heated under reflux for 7 h. The solvent was removed and the precipitate was collected and recrystallized from ethanol to obtain the titled hydrazone as yellow crystals

with m.p = 208–209 °C. IR (KBr): (C = O amide 1647 cm<sup>-1</sup>), (= C-H aromatic 3033 cm<sup>-1</sup>), (NH 3195 cm<sup>-1</sup>), (C = N 1591 cm<sup>-1</sup>). <sup>1</sup>H NMR (400 MHz, DMSO): δ = 2.9 (s, 6H, -N(CH<sub>3</sub>)<sub>2</sub>), 6.7–8.7 (m, 8H, aromatic protons), 8.3 (s, 1H, -C = N), 11.7 (s, 1H, -NH). <sup>13</sup>C-NMR δ = 38 (2CH<sub>3</sub>), 112–152 (11 aromatic carbons in two rings), 161 (C = O amide), 145 (C = N).

Synthesis of N'-[(3Z)-2-oxo-1,2-dihydro-3H-indol-3-ylidene]pyridine-4-carbohydrazide (OHEI): A mixture of 0.01 mmol isoniazide (1) with 0.01 mmol of Isatin with a catalytic amount of glacial acetic acid was refluxed for 8 h. The precipitate which is formed was collected and washed with ethanol then recrystallized from DMF to afford the titled hydrazone as an orange powder with m.p ≥ 295 °C. IR(KBr): (C = O amide 1669 cm<sup>-1</sup>), (C = O cyclic amide 1694 cm<sup>-1</sup>), (NH 3224 cm<sup>-1</sup>), (NH cyclic 3157 cm<sup>-1</sup>), (C = N 1616 cm<sup>-1</sup>). <sup>1</sup>H NMR (400 MHz, DMSO): δ = 7.3–8.7 (m, 8H, aromatic protons in indole and pyridine nucleus), 10.9 (s, 1H, -NH). <sup>13</sup>C-NMR δ = 112–152 (11 aromatic carbons in indole and pyridine), 163 (C = O amide), 162 (C = O amide), 132 (C = N).

## 2.2. Gravimetric Experiments

To extract the values of the N80 steel corrosion rate, the gravimetric procedure was carried out following the approved standard “ASTM G 31–72” [28]. The samples were immersed in a Pyrex glass cell, in an aerated medium comprising the corrosive solution elaborated in the absence and presence of the two inhibitors of the isonicotinohydrazide family, i.e., MAPEI and OHEI at a temperature of 303 K and 363 K at an immersion time of 24 h. These tests were repeated three times for all tested concentrations: 10<sup>-4</sup>, 5 × 10<sup>-4</sup>, 10<sup>-3</sup>, and 5 × 10<sup>-3</sup> mol/L. The corrosion rate  $C_R$  in (mm y<sup>-1</sup>) of each sample was obtained from the following Equation (1):

$$C_R \left( \text{mm y}^{-1} \right) = \frac{K \times \Delta W}{A \times \rho \times t} \quad (1)$$

where  $\Delta W$  is the mass in ±1 mg;  $t$  is the exposure time in ±0.01 h;  $A$  is the sample area in ±0.01 cm<sup>2</sup>;  $\rho$  is the metal density in g/cm<sup>3</sup>; and  $K = 8.67 \times 10^4$  is a conversion factor. The corrosion inhibition efficiency  $\eta\%$  of tested compounds and their degree of surface coverage ( $\theta$ ) were determined using the average corrosion rate, by following Equations (2) and (3) [29]:

$$\eta = \frac{C_R^0 - C_R^{Inh}}{C_R^0} \times 100 \quad (2)$$

$$\theta = \frac{\eta}{100} \quad (3)$$

where  $C_R^0$  and  $C_R^{Inh}$  are the non-inhibited and inhibited corrosion rates, respectively.

## 2.3. Electrochemical Measurements

To perform electrochemical analysis, an 80 mL Pyrex glass cell with a circulating water thermostat to keep the electrolyte at a temperature of 303 K was used. A reference electrode of saturated calomel (SCE), an auxiliary electrode of platinum, and N80 steel as the working electrode were used to constitute the three-electrode cell controlled by Volta Lab PGZ 100 instrument (Radiometer Analytical, Shanghai, China) and monitored by VoltaMaster 4.0 software. Before carrying out measurements, the working electrode was immersed in inhibited and blank solutions for a time of 120 min until the open circuit potential (OCP) reaches a steady state. Then, the non-destructive electrochemical impedance analyses were carried out under the same conditions, obtaining impedance curves in frequency values between 100 kHz and 10 mHz with the use of AC signals with 10 steps for each decade. Polarization tests in the potentiodynamic mode were performed with a scanning speed of 0.1667 mV/s [30,31]; this speed gives very efficient results in a quasi-stationary state. Potentiodynamic polarization curves in a potential range between -700 mV/SCE and -200 mV/SCE. To obtain well-validated values, we repeated these analyses three times.

Electrochemical data were analyzed with the help of Z-View 2 (Scribner Associates Inc, Southern Pines, NC, USA) and EC-Lab demo software (BioLogic, Seyssinet-Pariset, France).

#### 2.4. Surface Characterization

A field emission scanning electron microscope (FE-SEM) was used to investigate the morphology of the N80 steel surface in the absence and presence of inhibitors. N80 steel specimens were immersed in 15 wt.% HCl without and with  $5 \times 10^{-3}$  mol/L of the best-performing inhibitor (MAPEI) for 24 h, then treated and dried before analysis. SEM was performed through an FE-SEM apparatus (MIRA3 module, TESCAN, Brno, Czech Republic) operating at 15 V.

#### 2.5. Theoretical Studies

##### 2.5.1. Quantum Chemical Parameters

To investigate the chemical reactivity and determine their theoretical parameters such as highest occupied molecular orbital (HOMO) and lowest unoccupied molecular orbital (LUMO) energies, a density functional theory calculation was performed. These parameters allow calculating other global reactivity parameters such as the electronegativity ( $\chi$ ), the ionization potential ( $IP$ ), the electron affinity ( $EA$ ), and the electron transfer fraction ( $\Delta N$ ) of the studied inhibitors (MAPEI and OHEI) according to the equations below. The Dmol3 code was used for all DFT calculations [32]. The conductor-like screening (COSMO) solvation module was used. The COSMO model, which is a popular continuum solvation model, incorporates solvation effects by using a scaled conductor instead of an exact dielectric boundary condition [33]. This approximation greatly simplifies the mathematical calculations and distinguishes COSMO from other solvation models. Additionally, COSMO utilizes Green's function as the dielectric operator, making it the first continuum solvation model to have analytical gradients and use a realistic cavity shape. The generalized gradient approximation (GGA) with the double polarization numerical basis set (DNP) was applied. All other parameters and convergence criteria were default values of "Fine" quality of Dmol<sup>3</sup> code. The following equations were used to determine the energy gap (Equation (4)),  $IP$ ,  $EA$ ,  $X$ ,  $\eta$ , and  $\Delta N$  values:

$$\Delta E_{gap} = E_{LUMO} - E_{HOMO} = IP - EA \quad (4)$$

$$IP = -E_{HOMO} \quad (5)$$

$$EA = -E_{LUMO} \quad (6)$$

$$X = \frac{IP + EA}{2} \quad (7)$$

$$\eta = \frac{E_{LUMO} - E_{HOMO}}{2} \quad (8)$$

$$\Delta N = \frac{\Phi_{Fe} - X_{inh}}{2 \times (\eta_{inh} + \eta_{Fe})} \quad (9)$$

where  $\Phi_{Fe} = 4.82$  eV, and the value of the total hardness  $\eta_{Fe}$  of iron is taken to be zero.

Local reactivity indices were used to examine the reactivity of each atom in molecules. To this end, the Fukui indices were analyzed and calculated using the following equations [34]:

$$f_k^+ = q_k(N + 1) - q_k(N) \quad (10)$$

$$f_k^- = q_k(N) - q_k(N - 1) \quad (11)$$

where  $q_k(N+1)$ ,  $q_k(N)$ , and  $q_k(N-1)$  are the electron densities on atom  $k$  corresponding to  $N+1$ ,  $N$ , and  $N-1$  electrons systems, respectively.

### 2.5.2. SCC-DFTB Simulations

SCC-DFTB was carried out within the framework of spin-polarized DFTB using the DFTB+ code [34]. The exchange-correlation energy was described within the generalized gradient approximation (GGA) parameterized by Perdew–Burke–Ernzerh (PBE) [35]. The empirical dispersion correction was used to accurately describe the effect of van der Waals (vdW) interactions [36]. The Slater–Koster trans3d DFTB parameters were used. SCC formalism with  $10^{-8}$  SCC tolerance, Broyden mixing scheme, and 0.01 smearing were used to speed up the convergence. All convergence thresholds were the default “Fine” quality values in the DFTB+ module. Monkhorst–Pack Brillouin zone k-point grids of  $(8 \times 8 \times 8)$  and  $(2 \times 2 \times 1)$  were used for the optimization calculation of the bulk lattice parameters and adsorption models, respectively. The initial lattice parameter of iron was 2.862 Å while the optimized one is 2.858 Å, confirming that selected methods and models were reasonable. It should be noted that for purely technical modeling reasons, results represented and discussed herein are for solid/vacuum interface. Therefore, this section focuses on the chemistry of the interactions between molecules and iron atoms to estimate the potential interactions and coordination properties.

The surface Fe(110) was built by constructing a periodic multi-slab model with a  $(5 \times 5)$  supercell and a vacuum spacing of 20 Å along the z-direction to account for spurious interactions between slabs. The molecules were placed on the top side of the slab. The two bottom-most atomic layers were fixed to bulk positions whereas all other degrees of freedom were allowed to relax. A cubic box of 30 Å in size was created for SCC-DFTB calculations of standalone molecules. Inkscape software was used for the post-processing of all figures. The total energies of isolated molecules (noted  $E_{\text{mol}}$ ), Fe(110) iron surface (noted  $E_{\text{surf}}$ ), and molecule/Fe(110) adsorption systems (noted  $E_{\text{mol/surf}}$ ) were used to determine the interaction energy as:

$$E_{\text{inter}} = E_{\text{mol/surf}} - (E_{\text{mol}} + E_{\text{surf}}) \quad (12)$$

## 3. Results and Discussion

### 3.1. Corrosion Rate Measurements

The gravimetric method allows the estimation of the corrosion rates of metallic materials and the performance of applied inhibitors. Herein, the effect of different concentrations of MAPEI and OHEI inhibitors on the corrosion rate of N80 steel in 15 wt.% HCl is investigated at 303 K and 363 K. Table 1 groups the weight loss results for N80 steel such as corrosion rate, surface coverage, and inhibition efficiency, while Figure 1a shows the relationship between these parameters (the variation of  $C_R$  corrosion rate and efficiency as a function of the concentration of the two inhibitors MAPEI and OHEI at 303 K). It should be noted that the corrosion rate value of the blank is in line with previously reported studies on the corrosion inhibition of N80 steel in 15 wt.% HCl [37,38]. On the other hand, from data in Figure 1a and Table 1, it can be observed that the corrosion rate  $C_R$  at 303 K decreases from 22 mm/year to a value of 0.88 mm/year and 1.98 mm/year for the compounds MAPEI and OHEI at  $5 \times 10^{-3}$  mol/L, respectively. This decrease in corrosion rate is attributed to the formation of a protective layer on the steel surface, mainly through the adsorption of inhibitors' molecules via heteroatoms such as N and O and aromatic rings [39–41]. In consequence, the corrosion inhibition of both compounds increases with increasing amounts of inhibitors, reaching maximum values at  $5 \times 10^{-3}$  mol/L. It increases from 85% and 82% at low concentrations to 96% and 91% for MAPEI and OHEI at an optimum concentration of  $5 \times 10^{-3}$  mol/L, respectively.

**Table 1.** Effect of MAPEI and OHEI concentrations on the corrosion data of N80 steel in 15% HCl at 303 K and 363 K.

Concentration (mol/L)	$C_R$ (mm/y)		$\eta$ (%)		$\Theta$	
	303 K	363 K	303 K	363 K	303 K	363 K
-	303 K	363 K	303 K	363 K	303 K	363 K
Blank	22 ± 1.8	1986	-	-	-	-
			MAPEI			
5 × 10 <sup>-3</sup>	0.88	236.4	96	88.1	0.96	0.88
1 × 10 <sup>-3</sup>	1.32	324.6	94	83.6	0.94	0.83
5 × 10 <sup>-4</sup>	2.42	648.3	89	67.3	0.89	0.67
1 × 10 <sup>-4</sup>	3.3	875.9	85	55.8	0.85	0.55
			OHEI			
5 × 10 <sup>-3</sup>	1.98	341.2	91	82.8	0.91	0.91
1 × 10 <sup>-3</sup>	2.86	458.6	87	76.9	0.87	0.87
5 × 10 <sup>-4</sup>	3.52	788.1	84	60.3	0.84	0.84
1 × 10 <sup>-4</sup>	3.96	1032	82	48.0	0.82	0.82

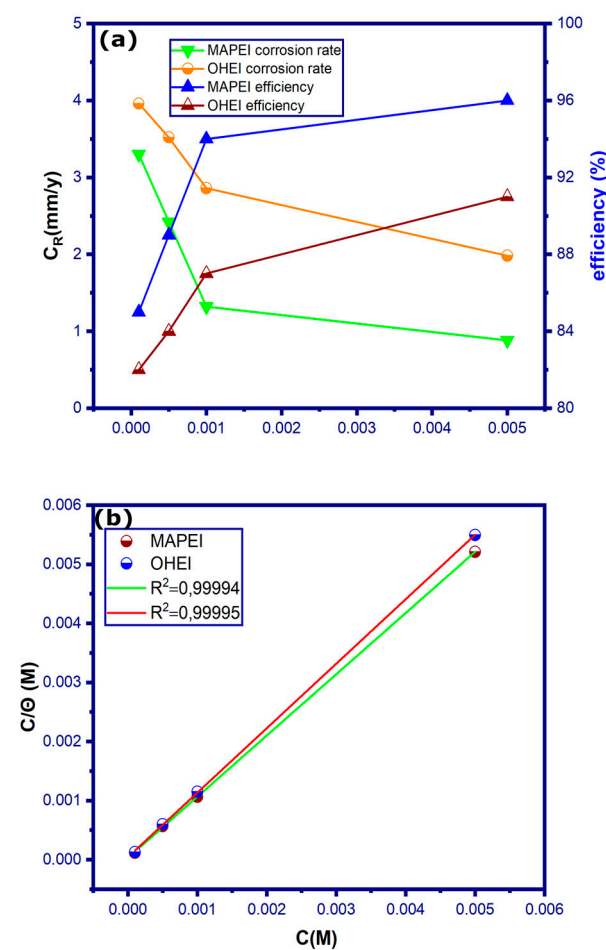
**Figure 1.** Relationship between corrosion rate, inhibition efficiency, and inhibitor concentrations for N80 steel after 24 h of immersion in 15 wt.% HCl inhibited with MAPEI and OHEI at 303 K (a) and Langmuir adsorption plots (b) for the adsorption of inhibitors on N80 steel surface.

Table 1 also shows the temperature effect on the inhibition efficiency of investigated compounds for N80 steel in 15 wt.% HCl solution. From the listed data, one can find that temperature has a significant effect on the inhibitors' performance. At the same inhibitor concentration, the inhibition efficiency decreases as the temperature increases from 303 K to 363 K. For instance, at 5 × 10<sup>-3</sup> mol/L of MAPEI, the corrosion rate decreases from 0.88 mm/y to 236.4 mm/y when the temperature increased from 303 K to 363 K, respectively. This decrease in corrosion inhibition performance at higher temperatures is found to be associated with the desorption of inhibitor molecules, leaving an increased

surface area of the metal exposed to the acid attack [42]. It should be pointed out that this behavior is common for organic corrosion inhibitors except for a few cases where the temperature has a positive effect on the inhibition efficiency [43,44]. However, one can notice that tested compounds maintain a relatively higher inhibition efficiency at higher concentrations. It suggests that there should be a strong chemical bonding between inhibitor molecules and the N80 steel, thus contributing to the stability of molecule adsorption [45].

From Figure 1b, which represents the variation of  $C/\theta$  as a function of the concentration of the two inhibitors MAPEI and OHEI at  $T = 303$  K, it can be noticed that the two lines are linear which implies that the adsorption of the two inhibitors on the surface of N80 steel in 15 wt.% HCl matches well the Langmuir isotherm model [46]. In corrosion inhibition studies, many previously published works use the fitting of isotherm models to experimental data to determine some thermodynamical parameters such as  $\Delta G_{ads}$  values, then making decisive conclusions about an inhibitor's adsorption mechanism on metal surfaces [47–50]. However, recent studies indicated that this approach is not always true and should be considered with strict precautions [51,52]. Therefore, adsorption isotherm data are not reported in the present studies and no decisive conclusions about adsorption mechanisms can be made based on adsorption isotherms [53–55].

### 3.2. Electrochemical Impedance Spectroscopy (EIS)

Electrochemical impedance spectroscopy is a very useful non-destructive analytical method that allows the characterization of electrochemical behavior and corrosion inhibition mechanism of various metal/electrolyte interfaces [56]. Figure 2 depicts the Nyquist and Bode curves. In the absence and presence of inhibitors, Nyquist curves contain imperfect single depressed capacitive loops with almost analogous forms, indicating no modification in the corrosion mechanism [57]. This analysis is supported by Bode curves (Figure 2a',b') which show a simple one-time constant model in the case of MAPEI while there is the appearance of a second time constant for higher concentrations of OHEI. Semicircle imperfections are frequently linked to the heterogeneity of steel surfaces. Though, as inhibitor concentrations rise, the width of semicircles grows noticeably, indicating that inhibitor molecules are adsorbing and forming a protective layer against HCl attack [58,59].

Impedance curves should be fitted by equivalent circuits for a thorough analysis of the corrosion inhibition process. Figure 2c,d shows the most suited electrical equivalent circuit obtained by fitting the investigative data. It contains solution resistance ( $R_s$ ), the constant phase element of the double layer ( $CPE_{dl}$ ), inhibitor film ( $CPE_f$ ), film resistance ( $R_f$ ), and polarization resistance ( $R_p$ ). The CPE is often used instead of capacitance to account for the non-ideal capacitive response from the interface. It is associated with the use of a solid electrode, in which the flattening is caused by a dispersion of frequency that is mainly attributed to roughness and inhomogeneities of the electrode surface [60,61]. All the fitted EIS data had Chi-squared values that are on the order of  $10^{-3}$ . Furthermore, the used electrical equivalent circuits have previously been found suitable to fit impedance data of N80 steel/15 wt.% HCl interfaces [62–65]. Equation (13) relates CPE to the impedance while Equation (14) determines double-layer capacitance values  $C_{dl}$ :

$$Z_{CPE} = \frac{1}{Q(j\omega)^n} \quad (13)$$

$$C_{dl} = \left( Q \times R_p^{1-n} \right)^{\frac{1}{n}} \quad (14)$$

where  $n$  and  $Q$  are the irregularity parameter and proportionality coefficient, respectively,  $j$  = imaginary unit, and  $\omega$  = angular frequency.

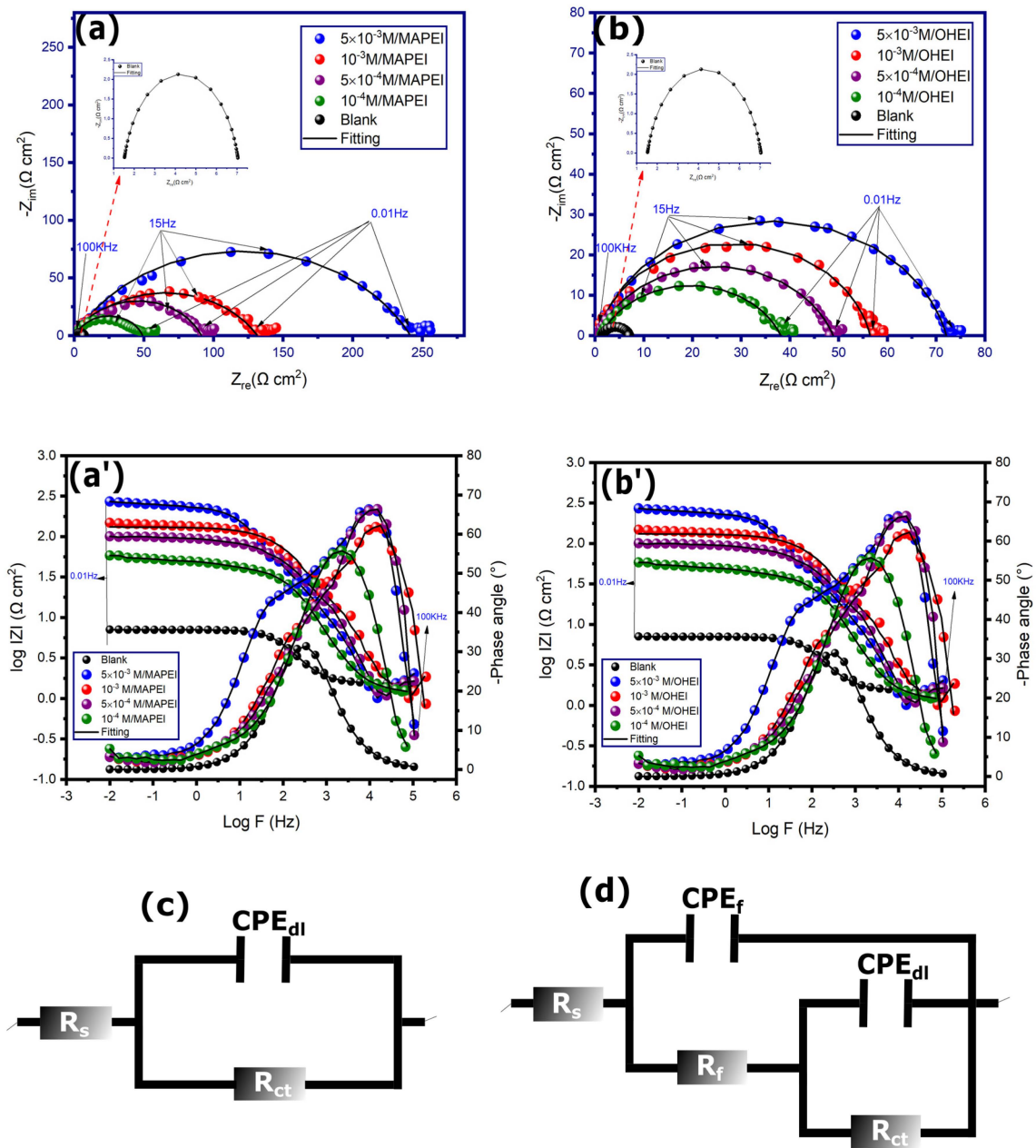


**Figure 2.** EIS data of N80 steel in 15% HCl with and without different concentrations of inhibitors; (a,a') Nyquist and Bode plots of MAPEI; (b,b') Nyquist and Bode plots of OHEI, respectively. (c,d) Equivalent electrical circuits used to fit EIS data.

Table 2 lists the inhibition efficiency  $\eta_{EIS}(\%)$  and other EIS parameters obtained by fitting impedance curves. The corrosion inhibition performance is evaluated by calculating the corrosion inhibition efficiency using the following equation:

$$\eta_{EIS}(\%) = \frac{R_p^{inh} - R_p^0}{R_p^{inh}} \times 100 \tag{15}$$

where  $R_p^{inh}$  and  $R_p^0$  represent the polarization resistance in the presence and absence of inhibitors, respectively.

**Table 2.** Electrochemical parameter values estimated according to EIS curves of N80 steel in 15 wt.% HCl solution in the presence and absence of several concentrations of MAPEI and OHEI at 303 K.

[Inhibitor] (mol/L)	$R_p = (R_f + R_{ct})$ ( $\Omega \text{ cm}^2$ )	$R_f$ ( $\Omega \text{ cm}^2$ )	$n$	$Q$ ( $\mu\text{F}/\text{cm}^2$ )	$C_{dl}$ ( $\mu\text{F cm}^{-2}$ )	$\eta_{EIS}$ (%)	Chi-Squared ( $\times 10^{-3}$ )
Blank	$5.51 \pm 1.3$	-	$0.83 \pm 0.004$	$697 \pm 1.353$	236		2.4
			MAPEI				
$5 \times 10^{-3}$	$241 \pm 1.2$	15	$0.69 \pm 0.006$	$89.14 \pm 2.08$	15	97.71	3.1
$1 \times 10^{-3}$	$131 \pm 1.6$	9	$0.65 \pm 0.003$	$165.12 \pm 1.9$	20	95.82	3.5
$5 \times 10^{-4}$	$91 \pm 1.9$	5	$0.74 \pm 0.005$	$207.44 \pm 1.7$	51	93.94	2.1
$1 \times 10^{-4}$	$48 \pm 1.7$	-	$0.78 \pm 0.002$	$229.54 \pm 2.1$	64	88.50	2.7
			OHEI				
$5 \times 10^{-3}$	$71 \pm 1.4$	-	$0.85 \pm 0.004$	$93 \pm 2.8$	38	92.30	4.5
$1 \times 10^{-3}$	$56 \pm 1.8$	-	$0.87 \pm 0.005$	$95 \pm 1.7$	43	90.15	3.8
$5 \times 10^{-4}$	$48 \pm 1.4$	-	$0.78 \pm 0.003$	$177 \pm 1.6$	46	88.59	4.2
$1 \times 10^{-4}$	$37 \pm 0.9$	-	$0.75 \pm 0.002$	$241 \pm 3.1$	49	85.07	5.4

The close inspection of data in Table 2 shows that the  $R_p$  value rises with the raise in the inhibitor concentrations, even in small concentrations  $1 \times 10^{-4}$  mol/L (47 and  $36 \Omega \text{ cm}^2$  for MAPEI and OHEI, respectively), compared to the 15 wt.% HCl solution ( $5.51 \Omega \text{ cm}^2$ ), signifying a protecting film formation over the surface of N80 steel. Furthermore, as the inhibitor concentration is increased, the magnitudes of  $C_{dl}$  values decrease, indicating that more organic molecules are adsorbed on the surface of N80 steel, replacing  $\text{H}_2\text{O}$  molecules, forming a thick barrier against the corrosive attack of HCl solution [66,67].

The impedance values rise with the addition of inhibitor concentrations in the estimated Bode curves ( $\log Z$  vs.  $\log f$  plot, Figure 2a',b'), indicating that the corrosion rate decreases in the presence of an inhibitor. In the case of the OHEI inhibitor, only the one-time constant assures that the process of charge transfer contains the process of single relaxation, according to the single wave phase angle–frequency plots (phase angle vs.  $\log f$ , Figure 1a'). However, two-time constants can be observed when increasing MAPEI concentrations are added to the HCl solution as indicated by the two points of inflection of the Bode phase plots in Figure 2b'. At high frequencies, the formed inhibitor film is represented by the  $R_f//CPE_f$  time constant, while the  $R_{ct}//CPE_{dl}$  characterizes the double layer formed at the metal/solution interface at low frequencies [68]. Due to the adsorption of inhibitor molecules, the Bode curves significantly increase in the presence of compounds. The capacitive electrochemical behavior of the N80 steel solution interface is specified by a rise in the phase angle value approaching  $70^\circ$ .

As observed in Table 2, the values of the polarization resistance  $R_p$  increase from  $5.51 \Omega \text{ cm}^2$  without inhibitors to  $241.1 \Omega \text{ cm}^2$  and  $71.59 \Omega \text{ cm}^2$  for MAPEI and OHEI inhibitors, respectively. This increase is due to the formation of an insulating protective film on the surface of N80 steel attributed to the decrease in the electrical double layer  $C_{dl}$  values because of inhibitors adsorption on the N80 steel surface [69]. Furthermore, the inhibition efficiency  $\eta_{EIS}(\%)$  increases from 88.5% and 85.07% to 97.71%, and 92.30% at  $5 \times 10^{-3}$  M of MAPEI and OHEI, respectively. This increase in  $\eta_{EIS}(\%)$  reflects the excellent adsorption properties of tested inhibitors, which is attributed to the presence of several reactive sites in their molecular structure such as heteroatoms N, O, and aromatic rings. Upon adsorption, these active sites would help create a strong inhibitor layer on the steel surface by charge transfer between the inhibitor's molecule and vacant  $d$ -orbitals of the steel surface [70].

### 3.3. Potentiodynamic Polarization Curves (PPC)

The potentiodynamic polarization curves allow the characterization of anodic and cathodic corrosion reactions of the steel surface in an HCl solution with and without inhibitors. Potentiodynamic polarization curves of N80 steel in the blank and inhibited 15 wt.% HCl solution are shown in Figure 3. Electrochemical parameters such as corro-

sion potential ( $E_{corr}$ ), corrosion current density ( $i_{corr}$ ), Tafel slopes ( $\beta_a$ ,  $\beta_c$ ), and inhibition efficiency ( $\eta_{PPC}\%$ ), which is calculated using Equation (16), are listed in Table 3:

$$\eta_{PDP}(\%) = \frac{i_{corr}^0 - i_{corr}^{inh}}{i_{corr}^0} \times 100 \quad (16)$$

where  $i_{corr}^0$  and  $i_{corr}^{inh}$  symbolize the corrosion current densities of N80 steel in blank reference and inhibited solutions, respectively.

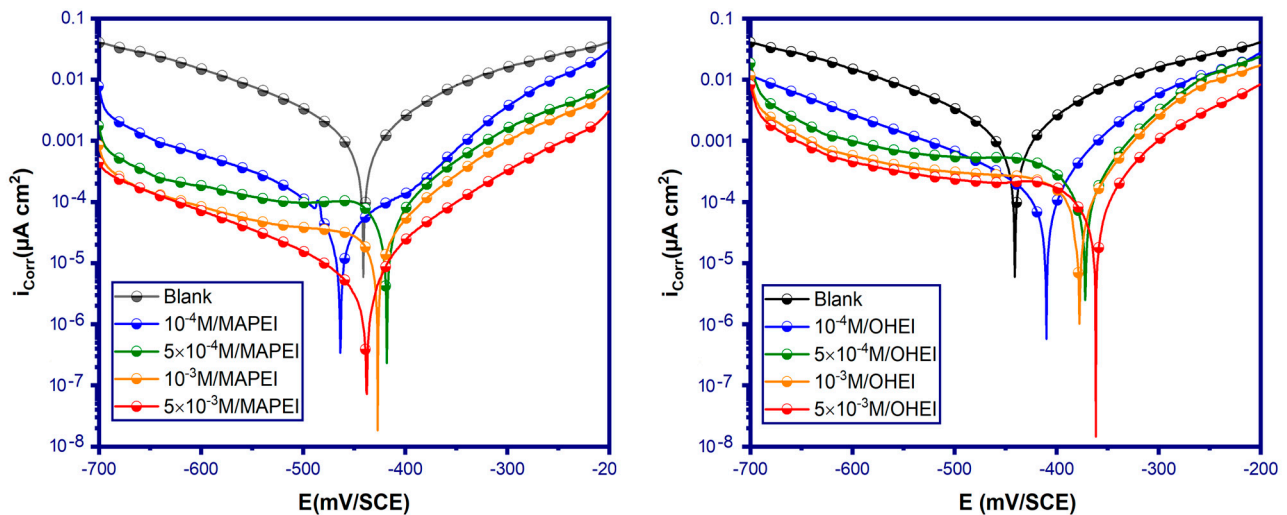


**Figure 3.** Potentiodynamic polarization curves of N80 steel in 15 wt.% HCl solution in the presence and absence of various concentrations of MAPEI and OHEI at 303 K.

**Table 3.** Electrochemical parameter values estimated from potentiodynamic polarization curves of N80 steel in 15 wt.% HCl solution without and with various concentrations of MAPEI and OHEI at 303 K.

Concentration (M)	$-E_{corr}$ (mV/SCE)	$\beta_c$ (mV/dec)	$-\beta_a$ (mV/dec)	$i_{corr}$ ( $\mu\text{A cm}^{-2}$ )	$\eta_{PPC}$ (%)
Blank	$440 \pm 0.5$	$111 \pm 4.3$	$48.67 \pm 3.2$	$1771 \pm 0.003$	-
MAPEI					
$5 \times 10^{-3}$	$437.909 \pm 0.3$	$179.051 \pm 4.2$	$92.90 \pm 2.9$	$76 \pm 0.005$	95.70
$1 \times 10^{-3}$	$426.975 \pm 0.6$	$181.402 \pm 3.8$	$101.19 \pm 3.7$	$116.91 \pm 0.007$	93.39
$5 \times 10^{-4}$	$417.957 \pm 0.8$	$182.94 \pm 4.2$	$119.59 \pm 3.3$	$210.68 \pm 0.004$	88.10
$1 \times 10^{-4}$	$463.3 \pm 0.9$	$185.97 \pm 4.1$	$97.29 \pm 3.1$	$287.96 \pm 0.008$	83.74
OHEI					
$5 \times 10^{-3}$	$362.557 \pm 0.2$	$659.29 \pm 3.9$	$97.17 \pm 2.8$	$132.47 \pm 0.002$	92.52
$1 \times 10^{-3}$	$372.62 \pm 0.9$	$687.18 \pm 4.3$	$89.48 \pm 3.2$	$254.85 \pm 0.001$	85.60
$5 \times 10^{-4}$	$372.19 \pm 0.6$	$693.64 \pm 3.9$	$95.72 \pm 3.5$	$310.53 \pm 0.005$	82.46
$1 \times 10^{-4}$	$373.74 \pm 0.7$	$685.79 \pm 4.5$	$96.21 \pm 3.1$	$327.75 \pm 0.003$	81.49

From PPC curves, it can be observed that the corrosion current densities of both anodic and cathodic reactions significantly decreased after adding an increasing amount of inhibitors MAPEI and OHEI. The significant reduction in anodic and cathodic branches is accompanied by a slight move of corrosion potential towards the anodic side. However, it is observed that each inhibitor's concentration has a different effect on the corrosion potential. Some added concentrations led to cathodic corrosion potentials while most of the inhibitors' concentrations led to more anodic corrosion potentials. This effect is more pronounced in the case of the OHEI compound. However, there is no obvious anodic shift of corrosion potential values. Furthermore, it is observed that there are no significant changes in the Tafel slope values upon the addition of compounds to the HCl solution, which means that both compounds have a mixed inhibition effect on both anodic and cathodic corrosion

reactions, with a more pronounced effect on the anodic reaction [71–74]. Table 3 shows that the  $\eta_{PPC}$  percentage increases from 83.70%, and 81.49% at  $10^{-4}$  mol/L to 95.70%, and 92.52% at a maximum concentration of  $5 \times 10^{-3}$  mol/L of MAPEI and OHEI, respectively. As shown from EIS data, this excellent inhibition effect results from the effective adsorption of inhibitor molecules on the N80 steel surface, forming a protective barrier that blocks anodic and cathodic corrosion reactions.

### 3.4. Immersion Time Effect

To be effective as corrosion inhibitors, organic compounds should have a high inhibition efficiency at low concentrations and long-term stability among other conditions. From electrochemical tests, it has been shown that tested compounds are effective at  $5 \times 10^{-3}$  mol/L. However, this performance must be assessed under long time tests before any further consideration for field testing. Given the fact that both inhibitors MAPEI and OHEI show similar corrosion inhibition behavior and high corrosion protection of N80 steel in 15 wt.% HCl at  $T = 303$  K, long-term tests are conducted only for the MAPEI compound. The effect of immersion times is performed for N80 steel in 15 wt.% HCl in the presence of  $5 \times 10^{-3}$  mol/L of MAPEI for an immersion period between 0.5 and 48 h at 303 K. Figure 4 shows the evolution of Nyquist and Bode EIS plots of N80 steel in 15 wt.% HCl inhibited with  $5 \times 10^{-3}$  mol/L of MAPEI over time while Table 4 lists the electrochemical parameters obtained by fitting impedance data using the electrical equivalent circuit in Figure 2. It can be seen that up to 36 h, the diameter of capacitive semicircles of Nyquist and Bode modulus values significantly increased reaching a high polarization value of around  $2805 \Omega \text{ cm}^2$ . Then it slightly decreased to around  $1450 \Omega \text{ cm}^2$  when the immersion time reaches 48 h. The excellent inhibition performance of the tested inhibitor at a longer immersion time is attributed to the increase in the adsorption of inhibitor molecules on the N80 steel surface creating a multilayer of inhibitor molecules and therefore maximizing the protection of its surface [75]. When the inhibitor's density on the steel surface increased, van der Waals interactions between interacting molecules would favor the desorption process, hence the stability of the formed inhibitor layer slightly decreased [76]. As 24 h is usually the needed time to ensure tubings' protection against corrosion, it can be concluded that the tested compound has excellent corrosion protection performance under studied conditions.

**Table 4.** Electrochemical parameter values estimated according to EIS curves of N80 steel in 15 wt.% HCl solution in the presence of  $5 \times 10^{-3}$  mol/L of MAPEI at 303 K at various immersion times.

Time (h)	$R_p$ ( $\Omega \text{ cm}^2$ )	$n$	$Q$ ( $\mu\text{F}/\text{cm}^2$ )	$C_{dl}$ ( $\mu\text{F cm}^{-2}$ )	Chi-Squared ( $\times 10^{-3}$ )
0.5	$241 \pm 1.2$	$0.69 \pm 0.006$	$89.14 \pm 2.08$	15	3.1
6	$633 \pm 1.8$	$0.68 \pm 0.007$	$65 \pm 2.11$	14.5	4.2
12	$1220 \pm 0.7$	$0.73 \pm 0.004$	$43 \pm 1.77$	14.4	3.7
24	$1870 \pm 2.1$	$0.69 \pm 0.005$	$42 \pm 2.31$	13.4	2.9
28	$3010 \pm 1.7$	$0.68 \pm 0.009$	$38 \pm 2.41$	13.7	1.8
36	$2805 \pm 1.3$	$0.68 \pm 0.008$	$37 \pm 1.65$	12.7	2.3
42	$2330 \pm 1.1$	$0.71 \pm 0.005$	$39 \pm 1.97$	14.6	2.7
48	$1450 \pm 1.4$	$0.72 \pm 0.007$	$38 \pm 1.86$	12.3	3.7

### 3.5. FE-SEM Analysis

SEM analysis is used to characterize the surface morphology of the N80 steel surface without and with the addition of  $5 \times 10^{-3}$  mol/L of MAPEI compounds under the same experimental conditions for 24 h of immersion. Figure 5 shows the N80 steel surface morphology in the blank (Figure 5a) and blank inhibited with  $5 \times 10^{-3}$  mol/L of MAPEI (Figure 5b). It can be seen from Figure 5a that in the absence of an inhibitor, the N80 steel has a degraded surface morphology with the existence of cavities and unstructured corrosive products. However, the morphology of N80 steel is significantly improved in the presence of the inhibitor as shown in Figure 5b. It is observed that the surface of the

N80 steel is smooth without corrosion attack due to the formation of a protective layer that blocks the corrosion attack.

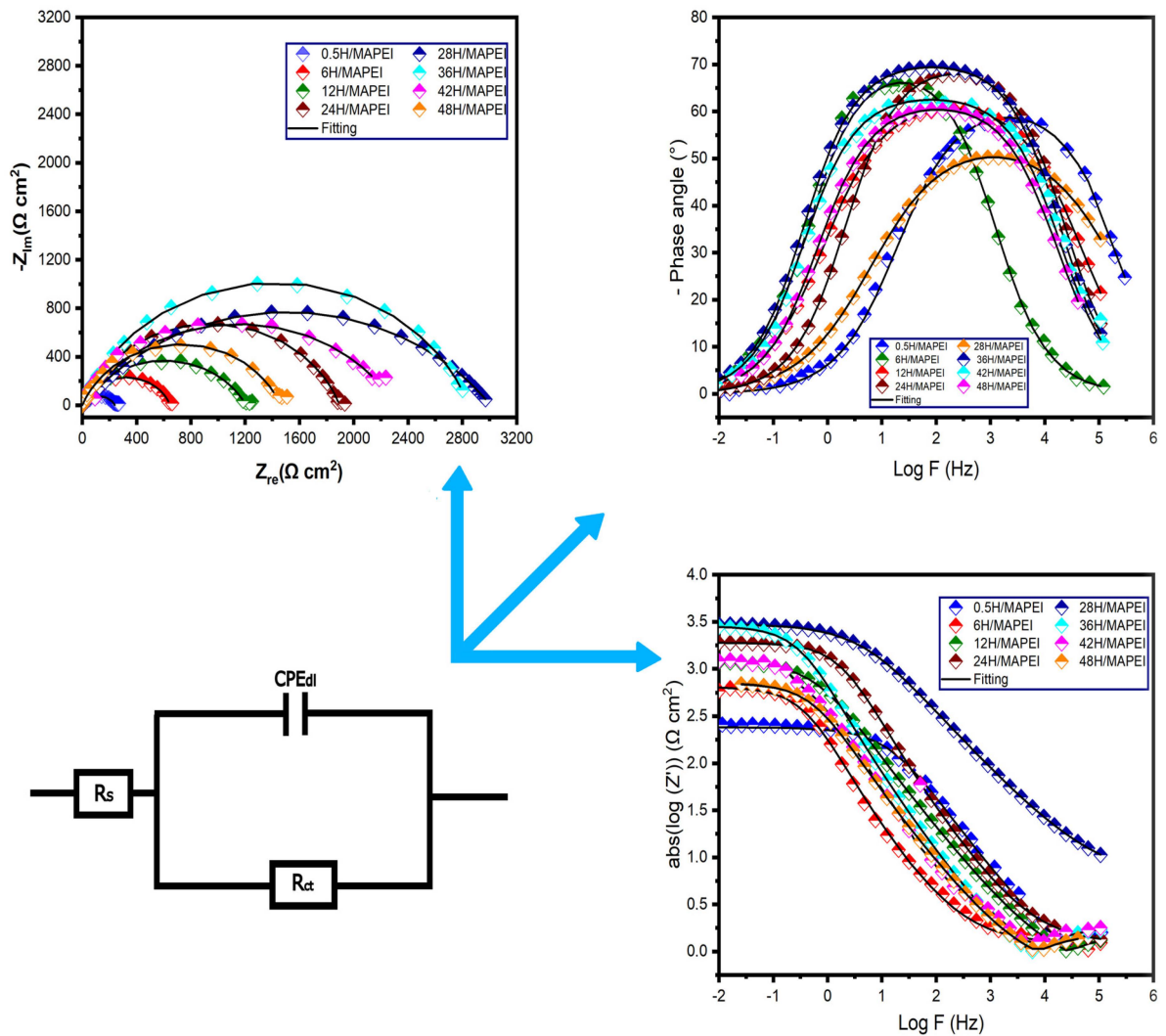


Figure 4. EIS and Bode diagrams of N80 steel substrate immersed in 15% HCl solution with  $5 \times 10^{-3}$  M of MAPEI at 303 K at various immersion times.

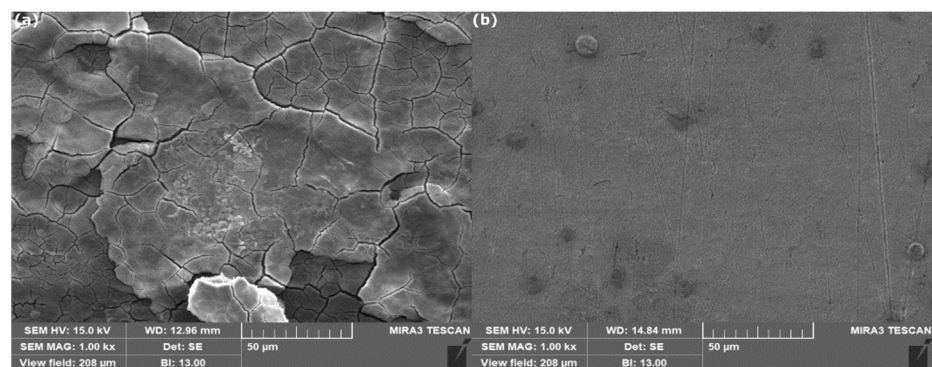
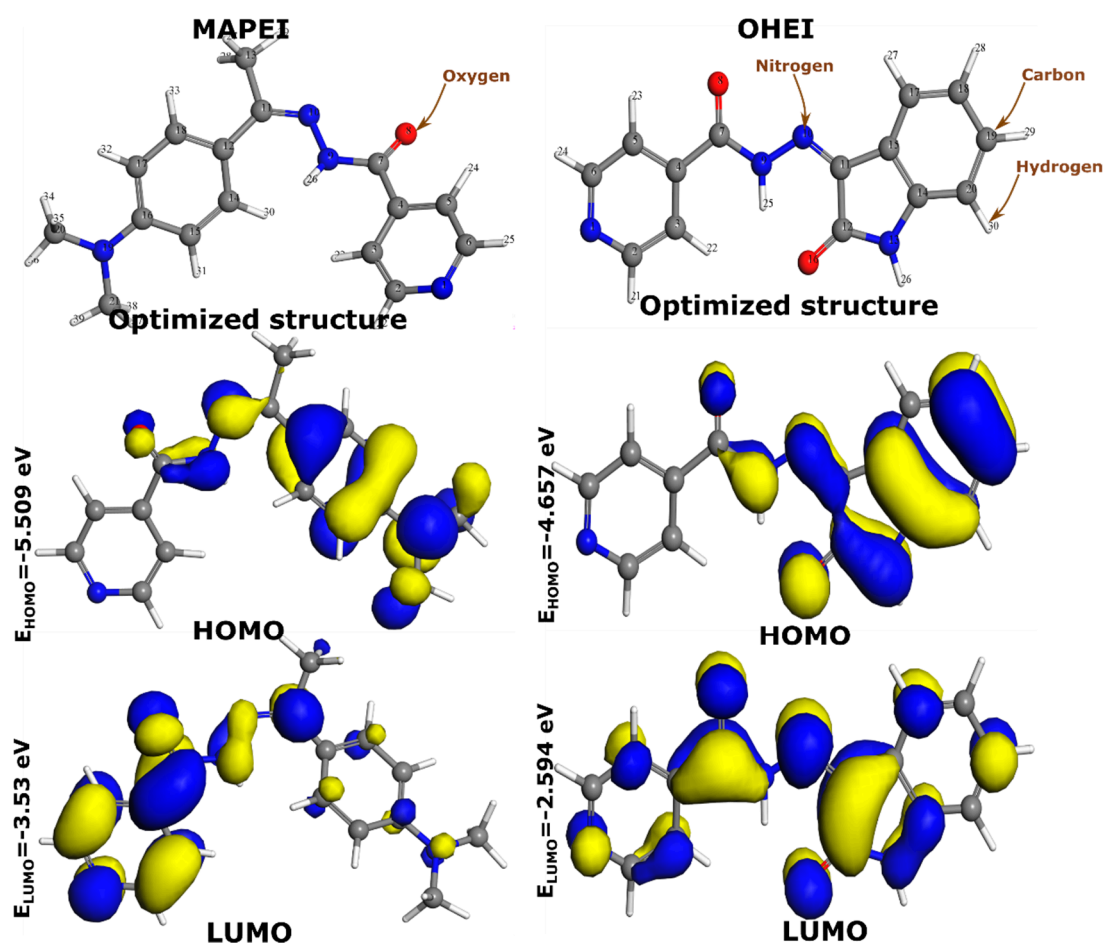


Figure 5. FE-SEM analysis of N80 steel surface in 15 wt.% HCl in the blank (a,b) inhibited acid solution with  $5 \times 10^{-3}$  mol/L of MAPEI.

### 3.6. Quantum Chemical Calculations

Recently, DFT calculations played a great role in corrosion inhibition research, because of their ability to reveal the reactivity of molecules and estimation of some quantum chemical parameters. Quantum chemical parameters can help understand the electronic properties of compounds thus getting insights into their ability to interact with other chemical species [77]. In this part, the global reactivity of the two inhibitor molecules MAPEI and OHEI and the local active sites of these molecules from the Fukui function indices are the main objectives. Figure 6 represents the optimized molecular structure, and frontier molecular orbitals, i.e., the highest occupied molecular orbital (HOMO), and the lowest unoccupied molecular orbital (LUMO). From HOMO and LUMO iso-surfaces, it can be observed that their electronic densities are distributed on the entire molecular structure of compounds covering almost all functional groups. It reveals that the entire molecule can participate in donor–acceptor interactions with other chemical species; particularly, investigated molecules containing several nitrogen-based functional groups and carbonyl groups which can act as preferred adsorption sites.



**Figure 6.** Optimized structures of MAPEI and OHEI molecules and their HOMO and LUMO iso-surfaces obtained at DFT-GGA-DNP level in the aqueous phase.

Table 5 gathers values of quantum chemical parameters of both MAPEI and OHEI. The HOMO and LUMO energies are related to the ability of a compound to donate and accept electrons, respectively [78]. Inspecting data in Table 5, one can notice that OHEI has a less negative HOMO energy while the MAPEI has a high negative LUMO energy value. It suggests that OHEI might be the compound with the highest electron-donating ability while the MAPEI with the highest electron-accepting tendency. However, it can be observed that both compounds have identical energy gap values. The energy gap is a

parameter that estimates the stability and reactivity of compounds. A compound with a high energy gap value is expected to have high stability and therefore less reactivity [78]. Given the identical values of the energy gap, both compounds are supposed to have similar reactivity and interactive force when interacting with other chemical species. Bearing these in mind, it must be noted that quantum chemical parameters are very limited in expecting the adsorption and performance of corrosion inhibitors as demonstrated by many recent studies [54,79].

**Table 5.** Calculated quantum chemical parameters of MAPEI and OHEI using DFT/GGA/DNP.

Molecules	$E_{HOMO}$ (eV)	$E_{LUMO}$ (eV)	$IP$ (eV)	$EA$ (eV)	$\Delta E_{gap}$ (eV)	$\chi$ (eV)	$\eta$ (eV)	$\Delta N_{110}$
MAPEI	−5.601	−3.539	5.601	3.539	2.062	4.57	1.03	2.6
OHEI	−4.657	−2.594	4.657	2.594	2.063	3.62	1.03	3.06

The reactivity of inhibitors can also be assessed using Fukui function indices. Fukui functions are a useful way to estimate the local reactivity of each atom of molecules, thus giving very close insights into their contribution when interacting with metal surfaces. The Fukui function can be used to identify the sites within the molecule that is available for nucleophilic and electrophilic attacks. Atomic sites, where the Fukui function is large, are softer and vice versa [80]. The electrophilic Fukui index  $f^+_k$  characterizes the sites for nucleophilic attacks. The nucleophilic Fukui index  $f^-_k$  describes preferred sites for attack by electrophiles [81,82].

Figure 7 represents the Fukui function indices of molecules under investigation. In Figure 7, it is obvious that atoms N(1), C(4)–C(7), and O(8) of MAPEI and C(7), O(8), N(10), C(11), C(12), and O(16) of OHEI exhibit the highest electrophilic Fukui index  $f^+_k$ , thus acting as preferred atomic sites to accept electrons during a nucleophilic attack [83]. On the other side, atoms C(12), C(15), C(17), and N(9) of MAPEI, and N(13), C(14), O(16), C(18) and C(19) of OHEI have the highest nucleophilic Fukui index  $f^-_k$ , suggesting that they are favorable sites for donating an electron to accepting species [83]. It can be noticed that the active sites are distributed over the entire molecular structure of the molecules with heteroatoms showing the most reactivity, and thus expected to have strong interactions with vacant d-orbitals of iron atoms.

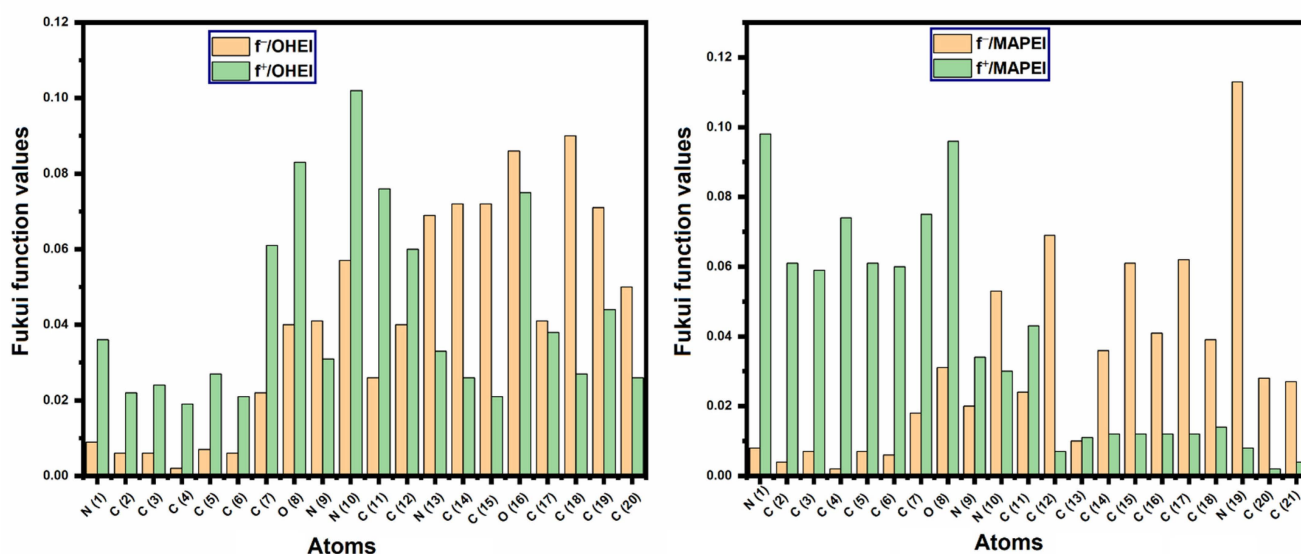


**Figure 7.** Graphical illustration of Fukui function indices of OHEI and MAPEI.

### 3.7. DFTB Calculations

#### 3.7.1. Adsorption Energy

It has been shown that investigated compounds have a strong affinity to steel surfaces, which is demonstrated by their excellent corrosion inhibition performance. The parallel adsorption configuration is found to be the most stable adsorption geometries of large-size organic compounds [84]. In the present section, DFTB simulations are carried out to simulate the interactions and binding of molecules with iron atoms. Figure 8 represents the adsorption geometry of MAPEI and OHEI on the Fe(110) surface. From quantum chemical analysis, it has been shown that inhibitor molecules have widespread active sites that can potentially interact with iron atoms. It can be observed from Figure 8 that MAPEI and OHEI molecules adopt a parallel adsorption mode on the surface of the metal, which signifies high adsorption affinities on the surface of iron [85]. Moreover, it can be noticed that both molecules can bind to iron atoms via carbon and heteroatoms. In the case of MAPEI, it forms four Fe-C bonds with bond length distances of 2.24–2.30 Å, and one Fe-O bond with a bond length distance of 2.22 Å. Concerning the OHEI molecule, five Fe-C bonds are formed with bond length distances of 2.16–2.31 Å and a single Fe-O bond with a bond length distance of 1.94 Å. The bonds resulting from the adsorption of molecules onto the iron surface have the following theoretical radius sums for Fe-C ( $r_C + r_{Fe}$ ) and Fe-O ( $r_O + r_{Fe}$ ) are 2.08 and 1.98 Å, respectively [86]. It indicates that bonds formed between inhibitor molecules and iron atoms are covalent bonds. The formation of several covalent bonds confirms the high reactivity of inhibitor molecules and their tendency to effectively interact with the iron surface. This has been shown from the analysis of quantum chemical parameters and Fukui functions indices, which showed the existence of several active sites that include both carbon and heteroatoms. The energetic evaluation of the adsorption geometries of both molecules gives an interaction energy of  $-2.78$  and  $-2.84$  eV for MAPEI and OHEI, respectively. It should be noted here that both molecules have high and approximately equal adsorption energies, due to similar structural properties and functional groups [87]. The presence of several electron donating groups with lone pairs such as  $-NCH_3$ ,  $-NH-$ , and  $-N =$  adjacent to and on  $\pi$ -systems would activate the aromatic ring by increasing the electron density on the ring through a resonance donating effect, thus generating more nucleophilic sites that would interact with electrophiles. This would also explain the dominant role of carbon atoms in bonding with iron atoms [88,89].

#### 3.7.2. Projected Density of States

To reveal the nature of the bonds and the potential charge transfer between the two molecules of MAPEI and OHEI and iron atoms, the projected density of states is determined. Figure 9 shows the plots of the projected density of states (PDOS) of adsorbed and isolated inhibitor molecules. In the adsorbed geometry, Figure 9a,b, it is observed that the molecular states between  $-5$  and  $5$  eV are significantly changed after the adsorption and formation of covalent bonds between inhibitor molecules and iron atoms. The peaks obtained for the isolated molecules in Figure 9c,d show peaks with high intensity and well-defined molecular states. However, after adsorption on the iron surface, these molecular peaks broadened slightly because of the hybridization interaction. The inhibitors' molecular orbitals will likely hybridize with metal  $d$ -states forming hybrid orbitals through the charge transfer process. As has been mentioned before, the presence of several heteroatoms and functional groups in the molecular structure of tested compounds promotes their adsorption on the iron surface. This high affinity to steel surfaces leads to excellent corrosion protection as shown by experimental studies.

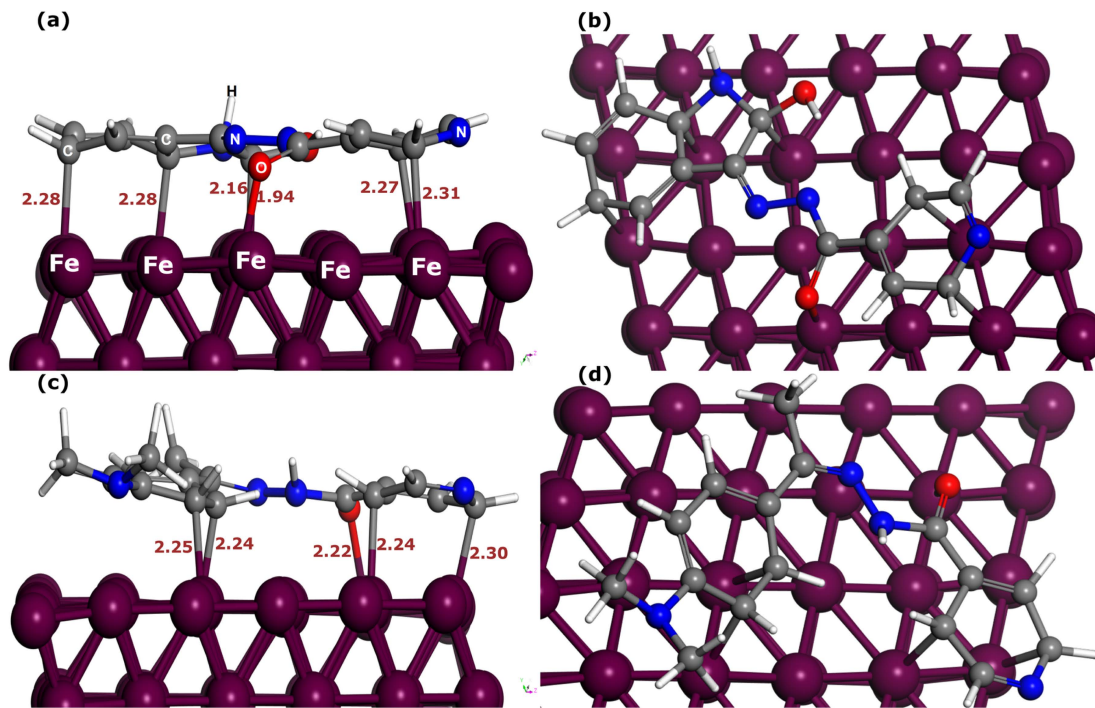


**Figure 8.** Optimized adsorption geometries of (a,b) OHEI and (c,d) MAPEI on Fe (110) surface obtained via DFTB calculations; (b,c): top views.

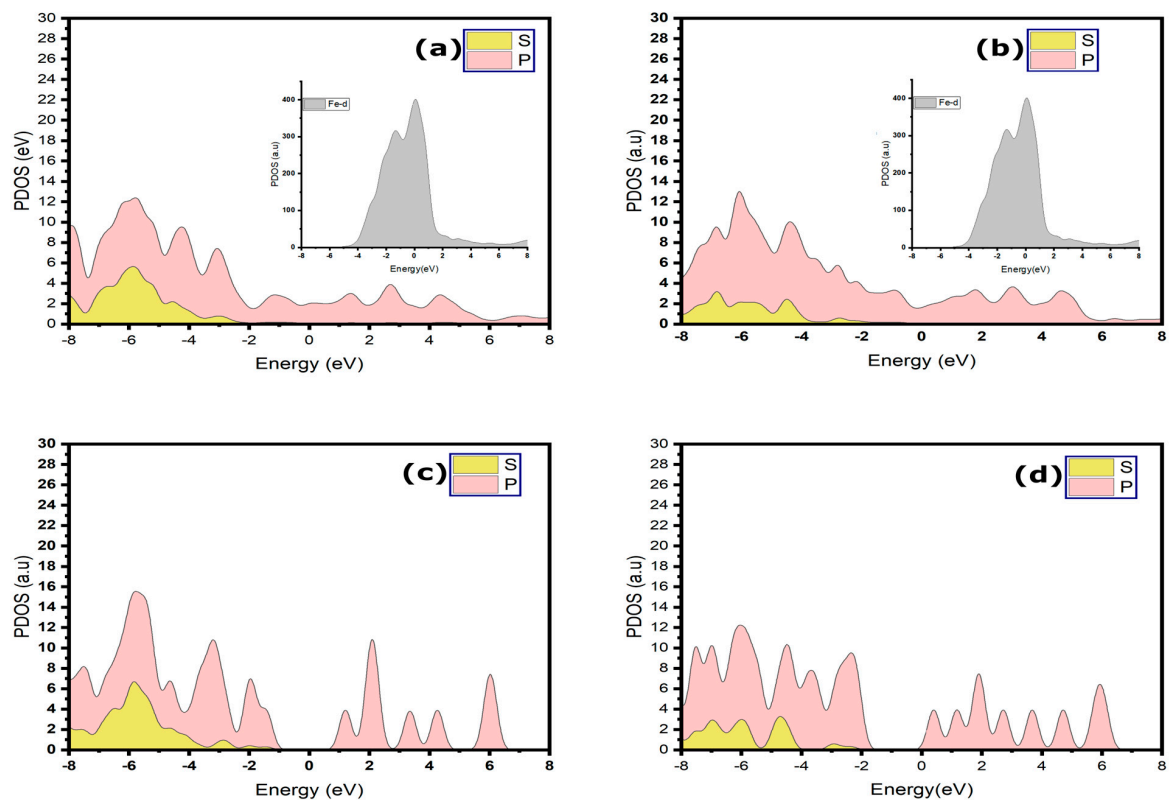


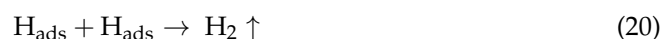
**Figure 9.** PDOS for (a) MAPEI, and (b) OHEI molecules adsorbed on Fe(110) surface and the Fe atoms beneath them (inset). (c,d) Isolated inhibitor molecules 7 Å above iron.

### 3.8. Corrosion Inhibition Mechanism

Experimental tests provided the first information on the corrosion inhibition performance of tested compounds, which mainly consists of controlling both anodic and cathodic corrosion reactions with a more effect on the anodic side and then establishing a barrier against the effects of corrosion as demonstrated from electrochemical results. In strongly acidic solutions such as 15 wt.% HCl, the hydrogen depolarization reaction is the main reason for anodic dissolution. The spontaneous dissolution of iron is accompanied by the corresponding cathodic reaction of hydrogen evolution as shown in Equations (17) and (18), respectively [90]:



The corrosion process is controlled by the hydrogen depolarization that occurs in two steps as follows [90]:



Experimental results from potentiodynamic polarization curves revealed that, without an inhibitor, hydrogen depolarization dominates at the cathodic sites, resulting in a strong dissolution of N80 steel in 15 wt.% HCl solution. While after adding an increasing amount of tested compounds, inhibitors form a protective barrier on the interface separating corrosive media from metal, leading to a significant decrease in the anodic dissolution and hydrogen evolution reaction [91–93]. On the other hand, it is found from impedance data that the polarization resistance increases due to the decrease in the thickness of the double-layer capacitance. It demonstrated the high ability of isonicotinohydrazide compounds to form a protective barrier on the surface of N80 steel in a concentrated acidic medium, i.e., 15 wt.% HCl. Furthermore, the DFTB method was used to explain and evaluate the interactions between the two inhibitor molecules and the iron surface. According to this theoretical approach, it has been found that inhibitor molecules coordinate chemically with the iron atoms by a charge transfer principle that is validated by the strong hybridization of the s- and p-states of the inhibitor molecules as evident in the PDOS plots. The carbonyl group atoms had a stronger affinity with the iron surface, while no covalent bonds were formed between the nitrogen atoms and the iron surface. Nitrogen atoms are most likely physically interacting with the iron surface via pre-adsorbed chloride ions that act as intermediates [94,95].

## 4. Conclusions

In the present study, the corrosion inhibition performance of newly synthesized isonicotinohydrazide compounds for N80 steel in 15 wt.% HCl using an experimental and theoretical approach. Electrochemical tests by electrochemical impedance spectroscopy and potentiodynamic polarization revealed a high corrosion protection ability of tested compounds with inhibition efficiencies reaching 97.71% and 92.30% for MAPEI and OHEI, respectively, at a concentration of  $5 \times 10^{-3}$  mol/L and  $T = 303$  K. Both inhibitors showed high corrosion inhibition properties thanks to the widespread active sites in their molecular structures. Furthermore, the MAPEI compound showed outstanding inhibition performance at a long immersion time of 48 h. FE-SEM analysis showed that the addition of MAPEI and OHEI inhibitors significantly improved the surface morphology of N80 steel immersed in 15 wt.% HCl. Quantum chemical calculations revealed that both molecules exhibited similar structural characteristics and chemical reactivity. When simulating their interactions with Fe(110) surface using DFTB simulation, inhibitor molecules were found to be very stable in the parallel adsorption mode, forming several covalent bonds with iron atoms. The analysis of adsorption geometries by PDOS revealed that inhibitor molecules co-

valently interact with iron atoms via a charge transfer process. The results from the present study demonstrate that compounds from isonicotinohydrazides can be very effective in protecting N80 steel in a highly corrosive medium of 15 wt.% HCl.

**Author Contributions:** Conceptualization, methodology, resources, supervision, validation, writing—review and editing, H.L., R.S., H.-s.L., I.H.A.; formal analysis, data curation, writing—original draft preparation, A.A.M., B.E.-H., R.J.A.; investigation, writing—review and editing, M.M., M.R.A., K.H. All authors have read and agreed to the published version of the manuscript.

**Funding:** Deanship of Scientific Research at King Khalid University; grant number R.G.P. 2/271/44.

**Data Availability Statement:** The data presented in this study are available on request from the corresponding author.

**Acknowledgments:** This work was supported by the Deanship of Scientific Research at King Khalid University for funding this work through the research groups program under grant number R.G.P. 2/271/44.

**Conflicts of Interest:** The authors declare no conflict of interest.

## References

1. Tait, W.S. Chapter 5—Electrochemical Corrosion Basics. In *Handbook of Environmental Degradation of Materials (Third Edition)*; Kutz, M., Ed.; William Andrew Publishing: Norwich, NY, USA, 2018; pp. 97–115. ISBN 978-0-323-52472-8.
2. Koch, G. 1—Cost of Corrosion. In *Trends in Oil and Gas Corrosion Research and Technologies*; El-Sherik, A.M., Ed.; Woodhead Publishing Series in Energy; Woodhead Publishing: Boston, MA, USA, 2017; pp. 3–30. ISBN 978-0-08-101105-8.
3. Hegazy, M.A.; El-Etre, A.Y.; El-Shafaie, M.; Berry, K.M. Novel Cationic Surfactants for Corrosion Inhibition of Carbon Steel Pipelines in Oil and Gas Wells Applications. *J. Mol. Liq.* **2016**, *214*, 347–356. [[CrossRef](#)]
4. Ansari, K.R.; Quraishi, M.A. Experimental and Computational Studies of Naphthyridine Derivatives as Corrosion Inhibitor for N80 Steel in 15% Hydrochloric Acid. *Phys. E Low-Dimens. Syst. Nanostruct.* **2015**, *69*, 322–331. [[CrossRef](#)]
5. Khalaf, M.M.; Tantawy, A.H.; Soliman, K.A.; Abd El-Lateef, H.M. Cationic Gemini-Surfactants Based on Waste Cooking Oil as New ‘Green’ Inhibitors for N80-Steel Corrosion in Sulphuric Acid: A Combined Empirical and Theoretical Approaches. *J. Mol. Struct.* **2020**, *1203*, 127442. [[CrossRef](#)]
6. Singh, A.; Ansari, K.R.; Quraishi, M.A.; Kaya, S. Theoretically and Experimentally Exploring the Corrosion Inhibition of N80 Steel by Pyrazol Derivatives in Simulated Acidizing Environment. *J. Mol. Struct.* **2020**, *1206*, 127685. [[CrossRef](#)]
7. El Azzouzi, M.; Azzaoui, K.; Warad, I.; Hammouti, B.; Shityakov, S.; Sabbahi, R.; Saoiabi, S.; Youssoufi, M.H.; Akartasse, N.; Jodeh, S.; et al. Moroccan, Mauritania, and Senegalese Gum Arabic Variants as Green Corrosion Inhibitors for Mild Steel in HCl: Weight Loss, Electrochemical, AFM and XPS Studies. *J. Mol. Liq.* **2022**, *347*, 118354. [[CrossRef](#)]
8. Palimi, M.j.; Tang, Y.; Wu, M.; Alvarez, V.; Ghavidel, M.; Kuru, E.; Li, Q.Y.; Li, W.; Li, D.Y. Improve the Tribo-Corrosion Behavior of Oil-in-Water Emulsion-Based Drilling Fluids by New Derivatives of Fatty Acid-Based Green Inhibitors. *Tribol. Int.* **2022**, *174*, 107723. [[CrossRef](#)]
9. Paul Setiawan Kaban, A.; Mayangsari, W.; Syaiful Anwar, M.; Maksun, A.; Riastuti, R.; Aditiyawarman, T.; Wahyuadi Soedarsono, J. Experimental and Modelling Waste Rice Husk Ash as a Novel Green Corrosion Inhibitor under Acidic Environment. *Mater. Today Proc.* **2022**, *62*, 4225–4234. [[CrossRef](#)]
10. Shojaee, S.; Shahidi Zandi, M.; Rastakhiz, N. The Effect of Tetracycline Drug as a Green Corrosion Inhibitor for Carbon Steel in HCl Media. *J. Indian Chem. Soc.* **2022**, *99*, 100700. [[CrossRef](#)]
11. Razizadeh, M.; Mahdavian, M.; Ramezanzadeh, B.; Alibakhshi, E.; Jamali, S. Synthesis of Hybrid Organic–Inorganic Inhibitive Pigment Based on Basil Extract and Zinc Cation for Application in Protective Construction Coatings. *Constr. Build. Mater.* **2021**, *287*, 123034. [[CrossRef](#)]
12. Shehnazdeep; Pradhan, B. A Study on Effectiveness of Inorganic and Organic Corrosion Inhibitors on Rebar Corrosion in Concrete: A Review. *Mater. Today Proc.* **2022**, *65*, 1360–1366. [[CrossRef](#)]
13. Lai, X.; Hu, J.; Ruan, T.; Zhou, J.; Qu, J. Chitosan Derivative Corrosion Inhibitor for Aluminum Alloy in Sodium Chloride Solution: A Green Organic/Inorganic Hybrid. *Carbohydr. Polym.* **2021**, *265*, 118074. [[CrossRef](#)]
14. Zhao, S.; Chen, K.; Zhang, L.; Yang, W.; Huang, D. Sulfonyl Hydrazides in Organic Synthesis: A Review of Recent Studies. *Adv. Synth. Catal.* **2020**, *362*, 3516–3541. [[CrossRef](#)]
15. Backes, G.L.; Neumann, D.M.; Jursic, B.S. Synthesis and Antifungal Activity of Substituted Salicylaldehyde Hydrazones, Hydrazides and Sulfohydrazides. *Bioorg. Med. Chem.* **2014**, *22*, 4629–4636. [[CrossRef](#)]
16. Kupski, O.; Funk, L.-M.; Sautner, V.; Seifert, F.; Worbs, B.; Ramsbeck, D.; Meyer, F.; Diederichsen, U.; Buchholz, M.; Schilling, S.; et al. Hydrazides Are Potent Transition-State Analogues for Glutaminyl Cyclase Implicated in the Pathogenesis of Alzheimer’s Disease. *Biochemistry* **2020**, *59*, 2585–2591. [[CrossRef](#)]

17. Yoshimatsu, M.; Ohta, K.; Takahashi, N. Propargyl Hydrazides: Synthesis and Conversion Into Pyrazoles Through Hydroamination. *Chem.—Eur. J.* **2012**, *18*, 15602–15606. [[CrossRef](#)]
18. Shetty, P. Hydrazide Derivatives: An Overview of Their Inhibition Activity against Acid Corrosion of Mild Steel. *S. Afr. J. Chem.* **2018**, *71*, 46–50. [[CrossRef](#)]
19. Varam, Y.; Rajkumari, L. Complexation Studies of N'-(1E)-1-Phenylethylidene]Isonicotinohydrazide: An Aroylhydrazone Schiff Base and Lanthanides. *J. Mol. Liq.* **2017**, *227*, 127–138. [[CrossRef](#)]
20. Dueke-Eze, C.U.; Madueke, N.A.; Iroha, N.B.; Maduelosi, N.J.; Nnanna, L.A.; Anadebe, V.C.; Chokor, A.A. Adsorption and Inhibition Study of N-(5-Methoxy-2-Hydroxybenzylidene) Isonicotinohydrazide Schiff Base on Copper Corrosion in 3.5% NaCl. *Egypt. J. Pet.* **2022**, *31*, 31–37. [[CrossRef](#)]
21. Abou-Melha, K. Synthesis, Characterization, and Biological Application of Some Transition Metal Complexes of N'-(Benzo[d][1,3]Dioxol-5-Ylmethylene)Isonicotinohydrazide. *J. Mol. Struct.* **2022**, *1268*, 133626. [[CrossRef](#)]
22. El-Lateef, H.M.A.; Soliman, K.A.; Al-Omair, M.A.; Adam, M.S.S. A Combination of Modeling and Experimental Approaches to Investigate the Novel Nicotinohydrazone Schiff Base and Its Complexes with Zn(II) and ZrO(II) as Inhibitors for Mild-Steel Corrosion in Molar HCl. *J. Taiwan Inst. Chem. Eng.* **2021**, *120*, 391–408. [[CrossRef](#)]
23. Iroha, N.B.; Dueke-Eze, C.U. Experimental Studies on Two Isonicotinohydrazide-Based Schiff Bases as New and Efficient Inhibitors for Pipeline Steel Erosion Corrosion in Acidic Cleaning Solution. *Chem. Afr.* **2021**, *4*, 635–646. [[CrossRef](#)]
24. Zaher, A.; Aslam, R.; Lee, H.-S.; Khafouri, A.; Boufellous, M.; Alrashdi, A.A.; El aoufir, Y.; Lgaz, H.; Ouhssine, M. A Combined Computational & Electrochemical Exploration of the *Ammi visnaga* L. Extract as a Green Corrosion Inhibitor for Carbon Steel in HCl Solution. *Arab. J. Chem.* **2022**, *15*, 103573. [[CrossRef](#)]
25. Gece, G. The Use of Quantum Chemical Methods in Corrosion Inhibitor Studies. *Corros. Sci.* **2008**, *50*, 2981–2992. [[CrossRef](#)]
26. Dehghani, A.; Bahlakeh, G.; Ramezanzadeh, B.; Ramezanzadeh, M. A Combined Experimental and Theoretical Study of Green Corrosion Inhibition of Mild Steel in HCl Solution by Aqueous Citrullus Lanatus Fruit (CLF) Extract. *J. Mol. Liq.* **2019**, *279*, 603–624. [[CrossRef](#)]
27. Lgaz, H.; Lee, H. Facile Preparation of New Hydrazone Compounds and Their Application for Long-Term Corrosion Inhibition of N80 Steel in 15% HCl: An Experimental Study Combined with DFTB Calculations. *J. Mol. Liq.* **2022**, *347*, 117952. [[CrossRef](#)]
28. Chafiq, M.; Thari, F.Z.; Lee, H.; Chaouiki, A.; Salghi, R.; Ko, Y.G.; Karrouchi, K.; Bougrin, K.; Ali, I.H.; Lgaz, H. Experimental and First-Principles DFT Insights into the Corrosion Protection Mechanism of Carbon Steel in an HCl Medium by Two Thiazolidinedione Compounds. *Mater. Today Commun.* **2022**, *32*, 103841. [[CrossRef](#)]
29. Chaouiki, A.; Chafiq, M.; Al-Moubaraki, A.H.; Bakhouch, M.; El Yazidi, M.; Gun Ko, Y. Electrochemical Behavior and Interfacial Bonding Mechanism of New Synthesized Carbocyclic Inhibitor for Exceptional Corrosion Resistance of Steel Alloy: DFTB, MD and Experimental Approaches. *Arab. J. Chem.* **2022**, *15*, 104323. [[CrossRef](#)]
30. Chaouiki, A.; Chafiq, M.; Rbaa, M.; Salghi, R.; Lakhrissi, B.; Ali, I.H.; Bashir, S.; Chung, I.-M. Comprehensive Assessment of Corrosion Inhibition Mechanisms of Novel Benzimidazole Compounds for Mild Steel in HCl: An Experimental and Theoretical Investigation. *J. Mol. Liq.* **2020**, *320*, 114383. [[CrossRef](#)]
31. Chafiq, M.; Chaouiki, A.; Albayati, M.R.; Lgaz, H.; Salghi, R.; AbdelRaheem, S.K.; Ali, I.H.; Mohamed, S.K.; Chung, I.-M. Unveiled Understanding on Corrosion Inhibition Mechanisms of Hydrazone Derivatives Based on Naproxen for Mild Steel in HCl: A Joint Experimental/Theoretical Study. *J. Mol. Liq.* **2020**, *320*, 114442. [[CrossRef](#)]
32. Quadri, T.W.; Olasunkanmi, L.O.; Fayemi, O.E.; Akpan, E.D.; Lee, H.-S.; Lgaz, H.; Verma, C.; Guo, L.; Kaya, S.; Ebenso, E.E. Multilayer Perceptron Neural Network-Based QSAR Models for the Assessment and Prediction of Corrosion Inhibition Performances of Ionic Liquids. *Comput. Mater. Sci.* **2022**, *214*, 111753. [[CrossRef](#)]
33. Klamt, A. *COSMO-RS: From Quantum Chemistry to Fluid Phase Thermodynamics and Drug Design*; Elsevier: Amsterdam, The Netherlands, 2005; ISBN 978-0-08-045553-2.
34. Fukui, K. The Role of Frontier Orbitals in Chemical Reactions (Nobel Lecture). *Angew. Chem. Int. Ed. Engl.* **1982**, *21*, 801–809. [[CrossRef](#)]
35. Perdew, J.P.; Burke, K.; Ernzerhof, M. Generalized Gradient Approximation Made Simple. *Phys. Rev. Lett.* **1996**, *77*, 3865. [[CrossRef](#)]
36. Grimme, S. Semiempirical GGA-Type Density Functional Constructed with a Long-Range Dispersion Correction. *J. Comput. Chem.* **2006**, *27*, 1787–1799. [[CrossRef](#)]
37. Kumar, S.; Sharma, D.; Yadav, P.; Yadav, M. Experimental and Quantum Chemical Studies on Corrosion Inhibition Effect of Synthesized Organic Compounds on N80 Steel in Hydrochloric Acid. *Ind. Eng. Chem. Res.* **2013**, *52*, 14019–14029. [[CrossRef](#)]
38. Solomon, M.M.; Umoren, S.A.; Quraishi, M.A.; Jafar Mazumder, M.A. Corrosion Inhibition of N80 Steel in Simulated Acidizing Environment by N-(2-(2-Pentadecyl-4,5-Dihydro-1H-Imidazol-1-yl) Ethyl) Palmitamide. *J. Mol. Liq.* **2019**, *273*, 476–487. [[CrossRef](#)]
39. Berrissoul, A.; Ouahach, A.; Benhiba, F.; Romane, A.; Guenbour, A.; Dikici, B.; Bentiss, F.; Zarrouk, A.; Dafali, A. Assessment of Corrosion Inhibition Performance of Origanum Compactum Extract for Mild Steel in 1 M HCl: Weight Loss, Electrochemical, SEM/EDX, XPS, DFT and Molecular Dynamic Simulation. *Ind. Crops Prod.* **2022**, *187*, 115310. [[CrossRef](#)]
40. Mehta, R.K.; Yadav, M.; Obot, I.B. Electrochemical and Computational Investigation of Adsorption and Corrosion Inhibition Behaviour of 2-Aminobenzohydrazide Derivatives at Mild Steel Surface in 15% HCl. *Mater. Chem. Phys.* **2022**, *290*, 126666. [[CrossRef](#)]

41. Zakaria, K.; Hamdy, A.; Abbas, M.A.; Abo-Elenien, O.M. New Organic Compounds Based on Siloxane Moiety as Corrosion Inhibitors for Carbon Steel in HCl Solution: Weight Loss, Electrochemical and Surface Studies. *J. Taiwan Inst. Chem. Eng.* **2016**, *65*, 530–543. [[CrossRef](#)]
42. Zhang, X.; Zheng, Y.; Wang, X.; Yan, Y.; Wu, W. Corrosion Inhibition of N80 Steel Using Novel Diquaternary Ammonium Salts in 15% Hydrochloric Acid. *Ind. Eng. Chem. Res.* **2014**, *53*, 14199–14207. [[CrossRef](#)]
43. Hou, B.S.; Zhang, Q.H.; Li, Y.Y.; Zhu, G.Y.; Lei, Y.; Wang, X.; Liu, H.F.; Zhang, G.A. In-Depth Insight into the Inhibition Mechanism of Pyrimidine Derivatives on the Corrosion of Carbon Steel in CO<sub>2</sub>-Containing Environment Based on Experiments and Theoretical Calculations. *Corros. Sci.* **2021**, *181*, 109236. [[CrossRef](#)]
44. Zhang, J.; Song, W.W.; Shi, D.L.; Niu, L.W.; Li, C.J.; Du, M. A Dissymmetric Bis-Quaternary Ammonium Salt Gemini Surfactant as Effective Inhibitor for Q235 Steel in Hydrochloric Acid. *Prog. Org. Coat.* **2012**, *75*, 284–291. [[CrossRef](#)]
45. Wang, X.; Yang, H.; Wang, F. A Cationic Gemini-Surfactant as Effective Inhibitor for Mild Steel in HCl Solutions. *Corros. Sci.* **2010**, *52*, 1268–1276. [[CrossRef](#)]
46. Chappell, M.; LeMonte, J.; McGrath, C.; Karna, R.; Styles, R.; Miller, C.; Miller, L.; Waites, M.; Middleton, M.; Price, C.; et al. Predicting Langmuir Model Parameters for Tungsten Adsorption in Heterogeneous Soils Using Compositional Signatures. *Geoderma* **2022**, *422*, 115924. [[CrossRef](#)]
47. Verma, C.; Olasunkanmi, L.O.; Ebenso, E.E.; Quraishi, M.A. Substituents Effect on Corrosion Inhibition Performance of Organic Compounds in Aggressive Ionic Solutions: A Review. *J. Mol. Liq.* **2018**, *251*, 100–118. [[CrossRef](#)]
48. Guo, L.; Tan, J.; Kaya, S.; Leng, S.; Li, Q.; Zhang, F. Multidimensional Insights into the Corrosion Inhibition of 3,3-Dithiodipropionic Acid on Q235 Steel in H<sub>2</sub>SO<sub>4</sub> Medium: A Combined Experimental and in Silico Investigation. *J. Colloid Interface Sci.* **2020**, *570*, 116–124. [[CrossRef](#)]
49. Tang, J.; Hu, Y.; Han, Z.; Wang, H.; Zhu, Y.; Wang, Y.; Nie, Z.; Wang, Y. Experimental and Theoretical Study on the Synergistic Inhibition Effect of Pyridine Derivatives and Sulfur-Containing Compounds on the Corrosion of Carbon Steel in CO<sub>2</sub>-Saturated 3.5 Wt.% NaCl Solution. *Molecules* **2018**, *23*, 3270. [[CrossRef](#)]
50. Dutta, A.; Saha, S.K.; Banerjee, P.; Sukul, D. Correlating Electronic Structure with Corrosion Inhibition Potentiality of Some Bis-Benzimidazole Derivatives for Mild Steel in Hydrochloric Acid: Combined Experimental and Theoretical Studies. *Corros. Sci.* **2015**, *98*, 541–550. [[CrossRef](#)]
51. Kokalj, A. Corrosion Inhibitors: Physisorbed or Chemisorbed? *Corros. Sci.* **2022**, *196*, 109939. [[CrossRef](#)]
52. Walczak, M.S.; Morales-Gil, P.; Lindsay, R. Determining Gibbs Energies of Adsorption from Corrosion Inhibition Efficiencies: Is It a Reliable Approach? *Corros. Sci.* **2019**, *155*, 182–185. [[CrossRef](#)]
53. Lavrich, D.J.; Wetterer, S.M.; Bernasek, S.L.; Scoles, G. Physisorption and Chemisorption of Alkanethiols and Alkyl Sulfides on Au(111). *J. Phys. Chem. B* **1998**, *102*, 3456–3465. [[CrossRef](#)]
54. Kokalj, A. Molecular Modeling of Organic Corrosion Inhibitors: Calculations, Pitfalls, and Conceptualization of Molecule–Surface Bonding. *Corros. Sci.* **2021**, *193*, 109650. [[CrossRef](#)]
55. Umoren, S.A.; Solomon, M.M.; Saji, V.S. Chapter 24—Mechanism of Corrosion Inhibition by Polymers. In *Polymeric Materials in Corrosion Inhibition*; Umoren, S.A., Solomon, M.M., Saji, V.S., Eds.; Elsevier: Amsterdam, The Netherlands, 2022; pp. 565–589. ISBN 978-0-12-823854-7.
56. Chafiq, M.; Chaouiki, A.; Lgaz, H.; Salghi, R.; Bhaskar, K.V.; Marzouki, R.; Bhat, K.S.; Ali, I.H.; Khan, M.I.; Chung, I.-M. Inhibition Performances of Spirocyclopropane Derivatives for Mild Steel Protection in HCl. *Mater. Chem. Phys.* **2020**, *243*, 122582. [[CrossRef](#)]
57. Aslam, R.; Mobin, M.; Aslam, J.; Lgaz, H.; Chung, I.-M. Inhibitory Effect of Sodium Carboxymethylcellulose and Synergistic Biodegradable Gemini Surfactants as Effective Inhibitors for MS Corrosion in 1 M HCl. *J. Mater. Res. Technol.-JMRT* **2019**, *8*, 4521–4533. [[CrossRef](#)]
58. Mobin, M.; Aslam, R. Experimental and Theoretical Study on Corrosion Inhibition Performance of Environmentally Benign Non-Ionic Surfactants for Mild Steel in 3.5% NaCl Solution. *Process Saf. Environ. Prot.* **2018**, *114*, 279–295. [[CrossRef](#)]
59. Zehra, S.; Mobin, M.; Aslam, J.; Parveen, M. Assessment of Glycine Derivative N-Benzylidene-2 ((2-Oxo-2-(10H-Phenothiazine-10yl) Ethyl) Amino) Acetohydrazide as Inhibitor for Mild Steel Corrosion in 1 M HCl Solution: Electrochemical and Theoretical Approach. *J. Adhes. Sci. Technol.* **2018**, *32*, 317–342. [[CrossRef](#)]
60. Pérez-Navarrete, J.-B.; Olivares-Xometl, C.O.; Likhanova, N.V. Adsorption and Corrosion Inhibition of Amphiphilic Compounds on Steel Pipeline Grade API 5L X52 in Sulphuric Acid 1 M. *J. Appl. Electrochem.* **2010**, *40*, 1605–1617. [[CrossRef](#)]
61. Sangeetha, Y.; Meenakshi, S.; Sairam Sundaram, C. Corrosion Inhibition of Aminated Hydroxyl Ethyl Cellulose on Mild Steel in Acidic Condition. *Carbohydr. Polym.* **2016**, *150*, 13–20. [[CrossRef](#)]
62. Umoren, S.A.; Solomon, M.M.; Obot, I.B.; Suleiman, R.K. Date Palm Leaves Extract as a Green and Sustainable Corrosion Inhibitor for Low Carbon Steel in 15 Wt.% HCl Solution: The Role of Extraction Solvent on Inhibition Effect. *Environ. Sci. Pollut. Res.* **2021**, *28*, 40879–40894. [[CrossRef](#)]
63. El-Haitout, B.; Selatnia, I.; Lgaz, H.; Al-Hadeethi, M.R.; Lee, H.-S.; Chaouiki, A.; Ko, Y.G.; Ali, I.H.; Salghi, R. Exploring the Feasibility of New Eco-Friendly Heterocyclic Compounds for Establishing Efficient Corrosion Protection for N80 Steel in a Simulated Oil Well Acidizing Environment: From Molecular-Level Prediction to Experimental Validation. *Colloids Surf. A Physicochem. Eng. Asp.* **2023**, *656*, 130372. [[CrossRef](#)]
64. Odewunmi, N.A.; Mazumder, M.A.J.; Ali, S.A.; Alharbi, B.G. Hydroquinone Decorated with Alkyne, Quaternary Ammonium, and Hydrophobic Motifs to Mitigate Corrosion of X-60 Mild Steel in 15 Wt.% HCl. *Chem.—Asian J.* **2021**, *16*, 801–821. [[CrossRef](#)]

65. Zhang, X.; Zhang, Y.; Su, Y.; Wang, X.; Lv, R. Synthesis and Corrosion Inhibition Performance of Mannich Bases on Mild Steel in Lactic Acid Media. *ACS Omega* **2022**, *7*, 32208–32224. [[CrossRef](#)] [[PubMed](#)]
66. Singh, A.; Ansari, K.R.; Quraishi, M.A.; Kaya, S.; Guo, L. Aminoantipyrine Derivatives as a Novel Eco-Friendly Corrosion Inhibitors for P110 Steel in Simulating Acidizing Environment: Experimental and Computational Studies. *J. Nat. Gas Sci. Eng.* **2020**, *83*, 103547. [[CrossRef](#)]
67. Solomon, M.M.; Umoren, S.A.; Quraishi, M.A.; Tripathy, D.B.; Abai, E.J. Effect of Akyl Chain Length, Flow, and Temperature on the Corrosion Inhibition of Carbon Steel in a Simulated Acidizing Environment by an Imidazoline-Based Inhibitor. *J. Pet. Sci. Eng.* **2020**, *187*, 106801. [[CrossRef](#)]
68. Haruna, K.; Saleh, T.A. Graphene Oxide with Dopamine Functionalization as Corrosion Inhibitor against Sweet Corrosion of X60 Carbon Steel under Static and Hydrodynamic Flow Systems. *J. Electroanal. Chem.* **2022**, *920*, 116589. [[CrossRef](#)]
69. Ansari, K.R.; Quraishi, M.A. Bis-Schiff Bases of Isatin as New and Environmentally Benign Corrosion Inhibitor for Mild Steel. *J. Ind. Eng. Chem.* **2014**, *20*, 2819–2829. [[CrossRef](#)]
70. Batah, A.; Chaouiki, A.; El Mouden, O.I.; Belkhaouda, M.; Bammou, L.; Salghi, R. Almond Waste Extract as an Efficient Organic Compound for Corrosion Inhibition of Carbon Steel (C38) in HCl Solution. *Sustain. Chem. Pharm.* **2022**, *27*, 100677. [[CrossRef](#)]
71. Jasim, A.S.; Rashid, K.H.; AL-Azawi, K.F.; Khadom, A.A. Synthesis of a Novel Pyrazole Heterocyclic Derivative as Corrosion Inhibitor for Low-Carbon Steel in 1M HCl: Characterization, Gravimetric, Electrochemical, Mathematical, and Quantum Chemical Investigations. *Results Eng.* **2022**, *15*, 100573. [[CrossRef](#)]
72. Lgaz, H.; Chung, I.-M.; Albayati, M.R.; Chaouiki, A.; Salghi, R.; Mohamed, S.K. Improved Corrosion Resistance of Mild Steel in Acidic Solution by Hydrazone Derivatives: An Experimental and Computational Study. *Arab. J. Chem.* **2020**, *13*, 2934–2954. [[CrossRef](#)]
73. Lgaz, H.; Saha, S.K.; Chaouiki, A.; Bhat, K.S.; Salghi, R.; Shubhalaxmi; Banerjee, P.; Ali, I.H.; Khan, M.I.; Chung, I.-M. Exploring the Potential Role of Pyrazoline Derivatives in Corrosion Inhibition of Mild Steel in Hydrochloric Acid Solution: Insights from Experimental and Computational Studies. *Constr. Build. Mater.* **2020**, *233*, 117320. [[CrossRef](#)]
74. Singh, A.; Ansari, K.R.; Alanazi, A.K.; Quraishi, M.A.; Ali, I.H.; Lin, Y. Probing Inhibition Effect of Novel Biopolymer Based Composite for the Inhibition of P110 Steel Corrosion in 15% HCl under Dynamic Condition. *Sustain. Chem. Pharm.* **2022**, *26*, 100599. [[CrossRef](#)]
75. Shahryari, Z.; Gheisari, K.; Yeganeh, M.; Ramezanzadeh, B. Corrosion Mitigation Ability of Differently Synthesized Polypyrrole (PPy-FeCl<sub>3</sub> & PPy-APS) Conductive Polymers Modified with Na<sub>2</sub>MoO<sub>4</sub> on Mild Steel in 3.5% NaCl Solution: Comparative Study and Optimization. *Corros. Sci.* **2021**, *193*, 109894. [[CrossRef](#)]
76. Njoku, D.I.; Okafor, P.C.; Lgaz, H.; Uwakwe, K.J.; Oguzie, E.E.; Li, Y. Outstanding Anticorrosion and Adsorption Properties of 2-Amino-6-Methoxybenzothiazole on Q235 and X70 Carbon Steels: Effect of Time, XPS, Electrochemical and Theoretical Considerations. *J. Mol. Liq.* **2021**, *324*, 114663. [[CrossRef](#)]
77. Guerrab, W.; Lgaz, H.; Kansiz, S.; Mague, J.T.; Dege, N.; Ansar, M.; Marzouki, R.; Taoufik, J.; Ali, I.H.; Chung, I.-M.; et al. Synthesis of a Novel Phenytoin Derivative: Crystal Structure, Hirshfeld Surface Analysis and DFT Calculations. *J. Mol. Struct.* **2020**, *1205*, 127630. [[CrossRef](#)]
78. Saha, S.K.; Dutta, A.; Ghosh, P.; Sukul, D.; Banerjee, P. Adsorption and Corrosion Inhibition Effect of Schiff Base Molecules on the Mild Steel Surface in 1 M HCl Medium: A Combined Experimental and Theoretical Approach. *Phys. Chem. Chem. Phys.* **2015**, *17*, 5679–5690. [[CrossRef](#)]
79. Kokalj, A.; Lozinšek, M.; Kapun, B.; Taheri, P.; Neupane, S.; Losada-Pérez, P.; Xie, C.; Stavber, S.; Crespo, D.; Renner, F.U.; et al. Simplistic Correlations between Molecular Electronic Properties and Inhibition Efficiencies: Do They Really Exist? *Corros. Sci.* **2021**, *179*, 108856. [[CrossRef](#)]
80. Obot, I.B.; Macdonald, D.D.; Gasem, Z.M. Density Functional Theory (DFT) as a Powerful Tool for Designing New Organic Corrosion Inhibitors. Part 1: An Overview. *Corros. Sci.* **2015**, *99*, 1–30. [[CrossRef](#)]
81. Bassey, I. Recent Advances in Computational Design of Organic Materials for Corrosion Protection of Steel in Aqueous Media. In *Developments in Corrosion Protection*; Aliofkhaezai, M., Ed.; InTech: Rijeka, Croatia, 2014; ISBN 978-953-51-1223-5.
82. Gómez, B.; Likhanova, N.V.; Domínguez-Aguilar, M.A.; Martínez-Palou, R.; Vela, A.; Gázquez, J.L. Quantum Chemical Study of the Inhibitive Properties of 2-Pyridyl-Azoles. *J. Phys. Chem. B* **2006**, *110*, 8928–8934. [[CrossRef](#)]
83. Pareek, S.; Jain, D.; Hussain, S.; Biswas, A.; Shrivastava, R.; Parida, S.K.; Kisan, H.K.; Lgaz, H.; Chung, I.-M.; Behera, D. A New Insight into Corrosion Inhibition Mechanism of Copper in Aerated 3.5 Wt.% NaCl Solution by Eco-Friendly Imidazopyrimidine Dye: Experimental and Theoretical Approach. *Chem. Eng. J.* **2019**, *358*, 725–742. [[CrossRef](#)]
84. Guo, L.; Qi, C.; Zheng, X.; Zhang, R.; Shen, X.; Kaya, S. Toward Understanding the Adsorption Mechanism of Large Size Organic Corrosion Inhibitors on an Fe(110) Surface Using the DFTB Method. *RSC Adv.* **2017**, *7*, 29042–29050. [[CrossRef](#)]
85. Machado Fernandes, C.; Guedes, L.; Alvarez, L.X.; Barrios, A.M.; Lgaz, H.; Lee, H.-S.; Ponzio, E.A. Anticorrosive Properties of Green-Synthesized Benzylidene Derivatives for Mild Steel in Hydrochloric Acid: An Experimental Study Combined with DFTB and Molecular Dynamics Simulations. *J. Mol. Liq.* **2022**, *363*, 119790. [[CrossRef](#)]
86. Cordero, B.; Gómez, V.; Platero-Prats, A.E.; Revés, M.; Echeverría, J.; Cremades, E.; Barragán, F.; Alvarez, S. Covalent Radii Revisited. *Dalton Trans.* **2008**, *37*, 2832–2838. [[CrossRef](#)] [[PubMed](#)]
87. Wu, L.; Han, Y.; Chen, S.; Li, W.; Shen, L. Study on the Structures and Electronic Properties of Double-Walled Silicon Nanotubes (4,Min)@(8,Mout) under External Electric Field by SCC-DFTB Calculations. *Comput. Mater. Sci.* **2022**, *202*, 110984. [[CrossRef](#)]

88. Thomas, A.; Prajila, M.; Shainy, K.M.; Joseph, A. A Green Approach to Corrosion Inhibition of Mild Steel in Hydrochloric Acid Using Fruit Rind Extract of *Garcinia Indica* (Binda). *J. Mol. Liq.* **2020**, *312*, 113369. [[CrossRef](#)]
89. Verma, C.; Quraishi, M.A.; Singh, A. A Thermodynamical, Electrochemical, Theoretical and Surface Investigation of Diheteroaryl Thioethers as Effective Corrosion Inhibitors for Mild Steel in 1 M HCl. *J. Taiwan Inst. Chem. Eng.* **2016**, *58*, 127–140. [[CrossRef](#)]
90. Popova, A.; Veleva, S.; Raicheva, S. Kinetic Approach to Mild Steel Corrosion. *React. Kinet. Catal. Lett.* **2005**, *85*, 99–105. [[CrossRef](#)]
91. Wang, H.; Liu, Y.; Xie, J.; Tang, J.; Duan, M.; Wang, Y.; Chamas, M. 3-(Diethylamino)-1-Phenylpropan-1-One as a Corrosion Inhibitor for N80 Steel in Acidization of Petroleum Exploitation. *Int. J. Electrochem. Sci* **2016**, *11*, 4943–4956. [[CrossRef](#)]
92. Hashim, N.Z.N.; Kahar, M.A.M.; Kassim, K.; Embong, Z.; Anouar, E.H. Experimental and Theoretical Studies of Azomethines Derived from Benzylamine as Corrosion Inhibitors of Mild Steel in 1 M HCl. *J. Mol. Struct.* **2020**, *1222*, 128899. [[CrossRef](#)]
93. Popova, A.; Christov, M.; Raicheva, S.; Sokolova, E. Adsorption and Inhibitive Properties of Benzimidazole Derivatives in Acid Mild Steel Corrosion. *Corros. Sci.* **2004**, *46*, 1333–1350. [[CrossRef](#)]
94. Solmaz, R. Investigation of Adsorption and Corrosion Inhibition of Mild Steel in Hydrochloric Acid Solution by 5-(4-Dimethylaminobenzylidene)Rhodanine. *Corros. Sci.* **2014**, *79*, 169–176. [[CrossRef](#)]
95. Solmaz, R. Investigation of Corrosion Inhibition Mechanism and Stability of Vitamin B1 on Mild Steel in 0.5M HCl Solution. *Corros. Sci.* **2014**, *81*, 75–84. [[CrossRef](#)]

**Disclaimer/Publisher’s Note:** The statements, opinions and data contained in all publications are solely those of the individual author(s) and contributor(s) and not of MDPI and/or the editor(s). MDPI and/or the editor(s) disclaim responsibility for any injury to people or property resulting from any ideas, methods, instructions or products referred to in the content.